

Analytical calculation of self-force effects on a scalar particle in an eccentric orbit around a Schwarzschild black hole

Salvatore Capozziello^{1,2,3,*}, Nicola Menadeo^{1,2,4,†} and Davide Usseglio^{1,2,‡}

¹*Scuola Superiore Meridionale, Largo San Marcellino 10, 80138, Naples, Italy*

²*INFN, Sezione di Napoli, Complesso Universitario di Monte S. Angelo, Via Cinthia Edificio 6, 80126, Naples, Italy*

³*Dipartimento di Fisica "E. Pancini", Università di Napoli "Federico II", Via Cinthia Edificio 6, I-80126, Napoli, Italy*

⁴*Max Planck Institute for Gravitational Physics (Albert Einstein Institute)
Am Mühlenberg 1, D-14476 Potsdam-Golm, Germany*

In this work, we analytically investigate the effects of the scalar self-force exerted by a massless scalar field on a particle in a slightly eccentric orbit around a Schwarzschild black hole. By solving the Klein-Gordon equation in the curved spacetime background, using a combination of post-Newtonian (PN) expansion, and small-eccentricity approximation, we derive explicit expressions for the self-force components at the particle location, as well as for the associated energy and angular momentum fluxes. Our results are valid up to sixth post-Newtonian (6PN) order and fourth order in eccentricity (e^4). We compare asymptotic fluxes with those obtained in [Phys. Rev. D 109, 104003 \(2024\)](#) for scalar-tensor (ST) theories. Once the relation between the two approaches has been established, we find perfect agreement by fixing the asymptotic value of the scalar field in ST theory $\phi_0 = 1$.

I. INTRODUCTION

The groundbreaking detection of gravitational waves (GWs) by the LIGO and Virgo collaborations [1, 2] opened a new avenue for investigating gravity in extreme regimes, particularly around black holes. This discovery has not only confirmed the theoretical foundations of General Relativity (GR), but also led to constraining a wide range of alternative gravity theories, many of which have been systematically ruled out [3, 4]. The next generation of GW observatories, including upgrades to current detectors and new facilities such as LISA, the Einstein Telescope and Cosmic Explorer [5–8], will significantly enhance the ability to detect potential deviations from GR [9–14].

One way to extend Einstein’s theory is to introduce an additional scalar field alongside the metric tensor. Depending on the nature of the coupling between the scalar field and the gravitational field, the scalar degree of freedom acts as a source term that does not change the underlying gravitational theory or it could lead to genuine modifications of the gravitational interaction, while preserving many of the fundamental symmetries of the original theory; this class of gravity models is known as Scalar–Tensor (ST) theories, in which gravity is mediated jointly by the usual spin-2 graviton and a spin-0 scalar mode. Over the years, such models have offered a flexible framework for probing deviations from standard GR, with applications mainly in the cosmological setting, i.e. for early (and late) time cosmic acceleration [15–21].

However, ST can also be employed in modeling astrophysical systems. In particular, there has been a revival in the investigation of ST theories in the gener-

ation of GWs from binary systems: among them, the Brans-Dicke (BD) model [22, 23] offers the simplest extension of GR by introducing a dynamical scalar field. In such a scenario, substantial efforts have been devoted to parametrize the impact of additional fields on observables, both analytically [24–33] and numerically [34, 35], with the aim of assessing whether such effects could be detectable in upcoming GW observations. These features could not only be due to a modification of the underlying gravitational theory, but they might also be interpreted as environmental effects on the binary, in which the scalar field plays the role of surrounding matter that interacts with the binary (see [36, 37]).

For the purpose of assessing the effects of scalar fields, intended either as a true modification to Einstein’s gravity or as an environmental effect, on the GW signal, Extreme Mass Ratio Inspiral (EMRI) events have emerged as powerful probes of fundamental physics [38–40], especially when analyzed within the sensitivity range of LISA [41–44]. EMRIs can be naturally investigated within the Self Force (SF) formalism [45, 46], where the central black hole of mass M , labeled *primary*, describes the background geometry, while the *secondary* object can be treated as a localized small perturbation of the background metric with mass μ , where $\mu/M \ll 1$.

In this work, we employ tools from Black Hole Perturbation Theory (BHPT) [45, 46], which provides a simplified yet insightful framework to study how the evolution of a scalar field is affected by the background geometry. Specifically, we focus on the Scalar Self-Force (SSF), which arises when a scalar charge interacts with its own field while moving along a prescribed trajectory. In this setup, we aim to analytically investigate the dynamics of a scalar particle in an equatorial, eccentric orbit around a Schwarzschild black hole, which has already been studied in [47] only via numerical techniques. Our calculations will be valid only at first order in $\mu/M \ll 1$, where μ is the mass of the scalar particle and M is the mass of the Schwarzschild black hole.

* capozziello@na.infn.it

† nicola.menadeo@aei.mpg.de

‡ davide.usseglio-ssm@unina.it

The ultimate goal of this analysis is to evaluate the components of the self-force. We then compute the scalar radiation via energy fluxes, which will provide a natural consistency check for our self-force calculation. Therefore, we neglect the backreaction of the scalar field on the background metric, as it would represent a higher-order effect in the perturbative expansion. In order to achieve this, we have to solve the differential equation governing the scalar field evolution, i.e. the spin- $s = 0$ Teukolsky equation, which, in the non-spinning case, reduces to the Klein-Gordon equation on a Schwarzschild background, sourced by a point-like particle. Similar setups have been widely explored in the gravitational self-force (GSF) context for $|s| = 2$ perturbations [48–50], including extensions to rotating black holes [51–53], and have provided valuable input for improving the Effective One Body (EOB) framework [54, 55]. Analytical calculations in this setting have also reached very high orders in small-eccentricity expansions [56–59].

The paper is organized as follows. In Sec. II we present a review of the eccentric orbits in Schwarzschild in the small eccentricity limit. We show explicit expressions for both the geodesic motion, periastron advance and radial orbital period. After these preliminaries, we provide a detailed discussion in Sec. III on how to solve the Klein-Gordon equation in the Schwarzschild background with a source that is forced to be on an eccentric orbit. We also provide a comparison of our results against the circular limit, by looking at the impact of the eccentricity at the various orders in the PN expansion. In Sec. IV we compute the SF components acting on the scalar particle, showing the differences compared to the circular limit. In Sec. V we complete our analytical computations with the evaluation of the asymptotic fluxes of energy and angular momentum, subsequently compared, in Sec. VI, with the scalar fluxes in Ref. [28] by establishing the correct mapping between the two sets of results.

As a side note, the Authors were surprised to note that analytical expressions for the scalar eccentric case were never investigated in detail in the literature, even in light of the recent interest mentioned in the previous paragraph. Another reason for this work was to close this gap.

Conventions. We use $G = c = 1$. We also use a placeholder $\eta = 1/c$ to clarify for the reader the nature of some PN series. Further, we use \log to indicate the natural logarithm. The signature for the Schwarzschild metric is $(-, +, +, +)$.

II. ECCENTRIC GEODESIC MOTION

Let us consider a Schwarzschild background geometry with the following line element

$$ds^2 = -f(r)dt^2 + \frac{dr^2}{f(r)} + r^2(d\theta^2 + \sin^2\theta d\phi^2), \quad (2.1)$$

in the usual set of Schwarzschild coordinates (t, r, θ, ϕ) and $f(r) = 1 - 2M/r$. Generic timelike trajectories $x^\mu = x_p^\mu(\tau)$ in the equatorial plane ($\theta = \pi/2$) can be parametrized in terms of the proper time τ .

According to these definitions, the components of the four-velocity $u^\mu = \dot{x}^\mu$ can be expressed in terms of the (specific) conserved energy E and angular momentum L as follows:

$$\dot{t}_p = \frac{E}{f(r_p)}, \quad \dot{r}_p^2 = E^2 - V(r_p, L), \quad \dot{\phi}_p = \frac{L}{r_p^2}, \quad (2.2)$$

where

$$V(r_p, L) = f(r_p) \left(1 + \frac{L^2}{r_p^2} \right), \quad (2.3)$$

and the dot indicates the derivative with respect to τ .

By solving the system in Eq. (2.2), we can write the components of the geodesic in terms of energy and angular momentum. However, since we are interested in eccentric orbits, it is more convenient to change the parameterization and to use the semi-latus rectum p and the (Darwin) eccentricity e by employing the expressions

$$E^2 = \frac{(p-2)^2 - 4e^2}{p(p-3-e^2)}, \quad L^2 = \frac{p^2 M^2}{p-3-e^2}, \quad (2.4)$$

where we recall that $p > 6 + 2e$ and $0 \leq e < 1$ for bound orbits.

With this set of variables, we can write the radial motion straightforwardly as

$$r_p(\chi) = \frac{Mp}{1 + e \cos \chi}, \quad (2.5)$$

with χ as the usual relativistic anomaly that takes values between 0 and 2π , which corresponds to the periastron and apoastron of the eccentric orbit. The geodesic equations can then be written in terms of the parameter χ as

$$\frac{d\phi}{d\chi} = \frac{\sqrt{p}}{\sqrt{p-6-2e \cos \chi}}, \quad (2.6a)$$

$$\frac{dt}{d\chi} = \frac{Mp^2}{(p-2-2e \cos \chi)(1+e \cos \chi)^2} \sqrt{\frac{(p-2)^2 - 4e^2}{p-6-2e \cos \chi}}, \quad (2.6b)$$

where the solutions for both equations can be written in terms of elliptic integrals, i.e.

$$\phi_p(\chi) = \left(\frac{4p}{p-6-2e} \right)^{1/2} F \left(\frac{\chi}{2} \middle| -\frac{4e}{p-6-2e} \right), \quad (2.7)$$

for the angular variable, with initial condition $\phi_p(0) = 0$. It is also possible to get a solution of this form for $t_p(\chi)$ but the procedure is more involved and it is not relevant for our discussion, though the expression can be found in [60]. Other representations for the solutions

of geodesic motion in the Schwarzschild spacetime can be found, see for instance [61, 62]. However, it is more useful to produce the geodesic periastron advance and the (radial) orbital period as

$$\Delta\phi = 2 \int_0^\pi d\chi \frac{d\phi}{d\chi} = \frac{4\sqrt{p}}{\sqrt{-6-2e+p}} \mathcal{K} \left(\frac{4e}{6+2e-p} \right) \quad (2.8)$$

$$\begin{aligned} \Delta T_r = 2 \int_0^\pi d\chi \frac{dt}{d\chi} = & C_1(p, e) \mathcal{K} \left(\frac{4e}{-6+2e+p} \right) \\ & + C_2(p, e) \mathcal{E} \left(\frac{4e}{-6+2e+p} \right) \\ & + C_3(p, e) \Pi \left(\frac{2e}{-1+e}, \frac{4e}{-6+2e+p} \right) \\ & + C_4(p, e) \Pi \left(\frac{4e}{-2+2e+p}, \frac{4e}{-6+2e+p} \right), \end{aligned} \quad (2.9)$$

where $\mathcal{E}(\cdot)$, $\mathcal{K}(\cdot)$ and $\Pi(\cdot)$ are the complete elliptic integrals of the first, second and third kind, respectively. Further, the C_i are rational functions of (p, e) .

Eccentric orbits have two fundamental frequencies which are associated with the libration between periastron and apoastron (Ω_r) and the average rate of azimuthal advance over one radial period (Ω_ϕ), which are respectively defined as

$$\Omega_r \equiv \frac{2\pi}{\Delta T_r}, \quad \Omega_\phi \equiv \frac{\Delta\phi}{\Delta T_r}. \quad (2.10)$$

Let us discuss how to obtain perturbative expressions for the aforementioned quantities. In particular, we are interested in the post-Newtonian (PN) approximation, which can be performed using $u_p = 1/p$ as PN expansion parameter. By implementing this expansion in the fundamental frequencies it is possible to check that $\Omega_r = \Omega_\phi$ at the Newtonian level. However, it is more convenient to use another counting parameter for the PN expansion, namely

$$y = (M\Omega_\phi)^{2/3}, \quad (2.11)$$

from which one can obtain the expression of p in terms of y by inverting the series in u_p of Ω_ϕ .

Once the PN expansion has been implemented on the various geodesic quantities, we also want to take into account a small eccentricity expansion. By expanding Eqs. (2.5) and (2.7), one finds

$$\begin{aligned} \frac{r_p(\chi)}{M} = & \frac{1}{y} - \frac{e \cos(\chi)}{y} - \frac{e^2}{y} [\sin^2(\chi) + P_2(y)] \\ & + \frac{e^3}{y} \cos(\chi) [\sin^2(\chi) + P_3(y)] \\ & + \frac{e^4}{8y} [\cos(4\chi) + P_4(y) + Q_4(y) \cos(2\chi)] + O(e^5), \end{aligned} \quad (2.12)$$

$$\begin{aligned} \phi_p(\chi) = & R_0(y)\chi + e R_1(y) \sin(\chi) \\ & + e^2 [R_2(y)\chi + S_2(y) \sin(2\chi)] \\ & + e^3 [R_3(y) \sin(\chi) + S_3(y) \sin(3\chi)] \\ & + e^4 [R_4(y)\chi + S_4(y) \sin(2\chi) + T_4(y) \sin(4\chi)], \end{aligned} \quad (2.13)$$

up to e^4 and where the $P_i(y)$, $Q_i(y)$, $R_i(y)$, $S_i(y)$ and $T_i(y)$ are polynomials in y that could be computed at arbitrary PN order. While the radial motion is explicitly periodic, the expression of $\phi_p(\chi)$ has also some linear-in- χ contributions which take into account that this quantity should not be periodic. It is useful to look at such a split also in the time domain expression for $\phi_p(t)$, which can be schematized as [63, 64]

$$\phi_p(t) = \Omega_\phi t + \Delta\phi(t), \quad (2.14)$$

where the first term represents the mean azimuthal advance, while the second is periodic over a radial period and, by reintroducing χ in this expression one gets

$$\begin{aligned} \Omega_\phi t(\chi) = & P'_0(y)\chi + e P'_1(y) \sin(\chi) \\ & + e^2 [P'_2(y)\chi + Q'_2(y) \sin(2\chi)] \\ & + e^3 [P'_3(y) \sin(\chi) + Q'_3(y) \sin(3\chi)] \\ & + e^4 [P'_4(y)\chi + Q'_{4,2}(y) \sin(2\chi) + Q'_{4,4}(y) \sin(4\chi)], \end{aligned} \quad (2.15a)$$

$$\begin{aligned} \Delta\phi(\chi) = & R'_1(y)e \sin(\chi) + R'_2(y)e^2 \sin(2\chi) \\ & + e^3 [R'_3(y) \sin(\chi) + S'_3(y) \sin(3\chi)] \\ & + e^4 [R'_4(y) \sin(2\chi) + S'_4(y) \sin(4\chi)], \end{aligned} \quad (2.15b)$$

which shows that the first line does not contain only linear-in- χ contributions but also some trigonometric functions, while the second line presents only $\sin(n\chi)$ with $|n| = 1, 2, 3, 4$. Again, we have introduced some polynomials in y to ease the notation and highlight the structure in χ . This separation in the time domain will turn out to be important in the next Section, where we will solve the Klein-Gordon equation sourced by a scalar charge on such orbits.

III. SCALAR FIELD IN ECCENTRIC MOTION AROUND A SCHWARZSCHILD BLACK HOLE

Let us now assume that a massless scalar field ψ , sourced by a scalar charge with mass $\mu \ll M$, is orbiting around the Schwarzschild black hole following an eccentric geodesic. The scalar field can then be modeled as a small perturbation to the Schwarzschild background, which obeys the spin-0 Teukolsky equation [65]. The equation reduces to the massless Klein-Gordon equation on a Schwarzschild background

$$\square\psi = 4\pi\rho, \quad (3.1)$$

where ρ is the charge density with support only along the particle world line

$$\rho(x^\mu) = q \int (-g)^{-1/2} \delta^{(4)}(x^\mu - x_p^\mu(\tau)) d\tau \quad (3.2)$$

and \square is a second-order differential operator defined as

$$\square = \frac{1}{\sqrt{-g}} \partial_\mu (\sqrt{-g} g^{\mu\nu} \partial_\nu). \quad (3.3)$$

By leveraging the spherical symmetry of the Schwarzschild background, the field ψ can be decomposed in terms of the (scalar) spherical harmonics $Y_{lm}(\theta, \phi)$ basis as follows

$$\psi(x^\mu) = \sum_{l,m} \psi_{lm}(t, r) Y_{lm}(\theta, \phi), \quad (3.4)$$

where we have separated the radial and the angular dependence¹. This allows us to solve the radial and the angular equations separately by keeping the indices (l, m) as parameters. Because we are interested in obtaining analytical expressions for $\psi(x^\mu)$, we need to expand each $\psi_{lm}(t, r)$ in Fourier series as

$$\psi_{lm}(t, r) = \sum_{n=-\infty}^{\infty} \psi_{lmn}(r) e^{-i\omega t}, \quad (3.5)$$

where $\omega \equiv \omega_{mn} = m\Omega_\phi + n\Omega_r$, which is a consequence of the bi-periodic motion of the source. The Fourier coefficients can be obtained by using standard definitions as

$$\psi_{lmn}(r) = \frac{1}{\Delta T_r} \int_0^{\Delta T_r} dt e^{i\omega t} \psi_{lm}(t, r). \quad (3.6)$$

Indeed, the same discussion can be done for the source term $\rho(x^\mu)$ to get the coefficients of the Fourier series $\rho_{lm}(t, r)$ as

$$\begin{aligned} \rho_{lmn}(r) &= \frac{q}{\Delta T_r E} Y_{lm}^* \left(\frac{\pi}{2}, 0 \right) \\ &\times \int_0^{\Delta T_r} dt \frac{f(r(t))}{r(t)^2} \delta(r' - r(t)) e^{i(\omega t - m\phi_p(t))}, \end{aligned} \quad (3.7)$$

where we derived the integrand from Eq. (3.2).

By using these mode-decomposed quantities, the equation for the scalar field $\psi_{lmn}(r)$ in Fourier space assumes the following form

$$\mathcal{L}_r \psi_{lmn} = -4\pi r^{-2} \rho_{lmn}, \quad (3.8)$$

where

$$\mathcal{L}_r \equiv \frac{d^2}{dr^2} + \frac{2(r-M)}{r^2 f(r)} \frac{d}{dr} + \left[\frac{\omega^2}{f(r)^2} - \frac{l(l+1)}{r^2 f(r)} \right], \quad (3.9)$$

¹ The equation under study is completely separable and the solutions to the angular equation are indeed the $Y_{lm}(\theta, \phi)$.

is a second-order differential operator.

The general inhomogeneous solution can be written for each (l, m) -modes as

$$\psi_{lmn}(r) = -4\pi \int dr' G_{lmn}(r, r') r'^2 \rho_{lmn}(r'), \quad (3.10)$$

where $G_{lmn}(r, r')$ is the Green function defined in terms of the homogeneous solutions

$$\begin{aligned} G_{lmn}(r, r') &= \frac{1}{W_{lmn}} [R_{\text{in}}^{lmn}(r) R_{\text{up}}^{lmn}(r') H(r' - r) \\ &+ R_{\text{in}}^{lmn}(r') R_{\text{up}}^{lmn}(r) H(r - r')], \end{aligned} \quad (3.11)$$

$H(\cdot)$ is the Heaviside step function, $R_{\text{in}}^{lmn}(r)$ and $R_{\text{up}}^{lmn}(r)$ are two independent homogeneous solutions of the radial equation with the correct boundary conditions at the event horizon of the Schwarzschild black hole and at infinity, respectively. Further, W_{lmn} is the invariant Wronskian

$$W_{lmn} = r^2 f(r) [R_{\text{in}}^{lmn}(r) R_{\text{up}}^{lmn}(r) - R_{\text{up}}^{lmn}(r) R_{\text{in}}^{lmn}(r)]. \quad (3.12)$$

By plugging Eq. (3.7) into Eq. (3.10) one has

$$\begin{aligned} \psi_{lmn}(r) &= -\frac{4\pi q}{\Delta T_r E} Y_{lm}^* \left(\frac{\pi}{2}, 0 \right) \int dr' G_{lmn}(r, r') r'^2 \\ &\times \int_0^{\Delta T_r} dt \frac{f(r(t))}{r(t)^2} \delta(r' - r(t)) e^{i(\omega t - m\phi_p(t))}, \end{aligned} \quad (3.13)$$

and the integration over r' becomes trivial because of the delta function, hence one gets

$$\begin{aligned} \psi_{lmn}(r) &= -\frac{4\pi q}{\Delta T_r E} Y_{lm}^* \left(\frac{\pi}{2}, 0 \right) \\ &\times \int_0^{\Delta T_r} dt G_{lmn}(r, r_p(t)) f(r(t)) e^{i(\omega t - m\phi_p(t))}. \end{aligned} \quad (3.14)$$

It is now convenient to recall the definition of ω in terms of the two fundamental frequencies of the eccentric motion and the time domain expression of $\phi_p(t)$ which leads to

$$\begin{aligned} \psi_{lmn}(r) &= -\frac{4\pi q}{\Delta T_r E} Y_{lm}^* \left(\frac{\pi}{2}, 0 \right) \\ &\times \int_0^{\Delta T_r} dt G_{lmn}(r, r_p(t)) f(r(t)) e^{i(n\Omega_r t - m\Delta\phi(t))}, \end{aligned} \quad (3.15)$$

and now, by changing the integration variable to χ as

$$\begin{aligned} \psi_{lmn}(r) &= -\frac{4\pi q}{\Delta T_r E} Y_{lm}^* \left(\frac{\pi}{2}, 0 \right) \\ &\times \int_0^{2\pi} d\chi \frac{dt}{d\chi} G_{lmn}(r, r_p(\chi)) f(r_p(\chi)) e^{i(n\Omega_r t - m\Delta\phi(\chi))}, \end{aligned} \quad (3.16)$$

it becomes clear that the integrand is periodic over an orbital cycle. One only has to perform the remaining integral, which is however very simple and involves only the integration of complex exponentials.

Once the integral is performed, there are three summations that need to be exploited: the sum over n which produces the time domain expression $\psi_{lm}(t, r)$, which is followed by the sums over (l, m) .

Since we are interested in a small eccentricity expansion, the infinite sum over n actually truncates at a finite number. In particular, at the specific order e^i , we have that the only non-zero terms of this sum are the ones with $|n| \leq i$. Besides, it is convenient to write the time domain (l, m) -modes of the field as

$$\begin{aligned}\psi_{lm}(t, r) &= e^{-im\Omega_\phi t} \sum_n \psi_{lmn}(r) e^{-in\Omega_r t} \\ &= e^{-im\Omega_\phi t} \bar{\psi}_{lm}(t, r),\end{aligned}\quad (3.17)$$

this choice will become clear in the next paragraphs.

The final steps involve the summation over (l, m) -modes but, more crucially, the evaluation of the time domain field $\psi(t, r, \theta, \phi)$ at the particle's position, i.e. $(r, \theta, \phi) \rightarrow (r_p(t), \pi/2, \phi_p(t))$. The resulting expression is, however divergent and must be suitably regularized through the mode-sum regularization [66, 67]. This method is well motivated, as Eq. (3.4) corresponds to the retarded field $\psi^{\text{ret}}(t, r, \theta, \phi)$, which is divergent at the particle location by construction, while its individual spherical-harmonic modes remain finite. The regularized field $\psi_R(t)$ can be thus computed by subtracting from each l -mode a suitable regulator $B(t)$ which does not depend on l .

The first step is to sum over m as

$$\begin{aligned}\psi_l^{\text{ret}}(t) &= \sum_{m=-l}^l \psi_{lm}(t, r) Y_{lm}(\theta, \phi) \Big|_{(r, \theta, \phi) \rightarrow (r_p(t), \pi/2, \phi_p(t))} \\ &= \sum_{m=-l}^l \bar{\psi}_{lm}(t, r) Y_{lm}(\pi/2, 0) e^{im\Delta\phi(t)} \Big|_{r \rightarrow r_p(t)},\end{aligned}\quad (3.18)$$

where the summation can be straightforwardly performed by using standard formulas (see Appendix F of

Ref. [68]). The retarded field is now explicitly periodic because the only non-periodic term produced by $e^{-im\Omega_\phi t}$ simplifies when the retarded field is evaluated at the particle position. Hence, the regular field is computed by subtracting the regulator *before* the summation over l

$$\psi_R(t) = \sum_l \{ \psi_l^{\text{ret}}(t) - B(t) \}.\quad (3.19)$$

To obtain explicit expressions for the regularized field, one must first express the Green function in terms of the homogeneous solutions $R_{\text{in}}^{lm\omega}(r)$ and $R_{\text{up}}^{lm\omega}(r)$ appearing in Eq. (3.11). The most straightforward approach consists in solving Eq. (3.8) expanding in PN and working out the equation order-by-order. This procedure yields what we refer to as the *PN solution*, which can be written for a generic l -mode. However, it does not satisfy the physical boundary condition at the horizon. This behaviour is reflected in the presence of some divergences at specific PN-order for certain values of l . To address this issue, the most commonly used technique is the so-called Mano-Suzuki-Takasugi method (MST) [69], which relies on writing the homogeneous solutions for the full equation in terms of an infinite sum of hypergeometric functions: these are referred to as the *MST solutions*. In practice, computing observables up to some $n_{\text{max}}\text{-PN}$, requires including all the MST solutions up to some $l \leq l_{\text{max}}^2$. The downside of this procedure is that each l -mode needs to be computed independently.

Besides, the MST solutions show an interesting analytical structure. In particular, the divergence in l of the PN solutions is translated in $\log(-i\omega r)$ which is indeed a problem in the high frequency limit. This is not a real issue for bound orbits, such as circular or eccentric, where the frequency spectrum is discrete and the large-frequency limit is never encountered in the calculation. A very different situation appears in the hyperbolic scattering case where the high frequency limit plays a crucial role and a suitable regularization procedure should be taken into account to extract physical quantities from the calculation (see Ref. [65]).

It is now possible to present the expressions for the parameter $B(\chi)$ and the regularized field, respectively; the periodic structure is well preserved at each order in e . Hence, up to 6PN and e^4 (in units of q)

$$\begin{aligned}B(y, e; \chi) &= y - \frac{y^2}{4} - \frac{39y^3}{64} - \frac{385y^4}{256} - \frac{61559y^5}{16384} - \frac{622545y^6}{65536} \\ &+ e \left(y - \frac{3y^2}{4} - \frac{99y^3}{64} - \frac{823y^4}{256} - \frac{110511y^5}{16384} - \frac{938331y^6}{65536} \right) \cos \chi \\ &+ e^2 \left[y - \frac{23y^2}{8} - \frac{15y^3}{2} - \frac{12677y^4}{512} - \frac{1758353y^5}{16384} - \frac{73637235y^6}{131072} \right]\end{aligned}$$

² The l_{max} can be deduced by looking at the coefficient in the PN solution of the specific order we are interested in and check for

which values of l it diverges. We identify the largest one as l_{max} .

$$\begin{aligned}
& - \left(\frac{3y^2}{8} + \frac{27y^3}{64} + \frac{93y^4}{512} - \frac{8001y^5}{8192} - \frac{612873y^6}{131072} \right) \cos 2\chi \Big] \\
& + e^3 \cos \chi \left[y - \frac{29y^2}{8} - \frac{129y^3}{16} - \frac{10387y^4}{512} - \frac{1154065y^5}{16384} - \frac{44917209y^6}{131072} \right. \\
& \quad \left. + \left(-\frac{y^2}{8} + \frac{21y^3}{64} + \frac{709y^4}{512} + \frac{27597y^5}{8192} + \frac{814491y^6}{131072} \right) \cos 2\chi \right] \\
& + e^4 \left[y - \frac{11y^2}{2} - \frac{7377y^3}{512} - \frac{95161y^4}{2048} - \frac{14850039y^5}{65536} - \frac{372021671y^6}{262144} \right. \\
& \quad \left. + \left(-\frac{3y^2}{4} + \frac{27y^3}{128} + \frac{3001y^4}{512} + \frac{494913y^5}{16384} + \frac{4559499y^6}{32768} \right) \cos 2\chi \right. \\
& \quad \left. + \left(\frac{45y^3}{512} + \frac{205y^4}{2048} - \frac{19305y^5}{65536} - \frac{510165y^6}{262144} \right) \cos 4\chi \right]. \tag{3.20}
\end{aligned}$$

The latter result has been computed by taking the PN solution of the Klein-Gordon equation for $l \rightarrow +\infty$. Besides, it is in agreement with the general expression for the B term computed in [70]. At this point, the explicit expression for the χ -domain regularized scalar field can also be provided, using the MST solutions up to $l = 4$ (included)

$$\begin{aligned}
\psi_{\text{R}}(y, e; \chi) = & -y^3 - \frac{38}{45}\pi y^{11/2} + y^4 \left(\frac{35}{18} - \frac{4\gamma_E}{3} - \frac{7\pi^2}{32} - \frac{4\log 2}{3} - \frac{2\log(y)}{3} \right) \\
& + y^5 \left(\frac{1141}{360} + \frac{2\gamma_E}{3} + \frac{29\pi^2}{512} - \frac{18\log 2}{5} + \frac{\log y}{3} \right) \\
& + y^6 \left(-\frac{23741}{1680} + \frac{77\gamma_E}{6} - \frac{279\pi^2}{1024} + \frac{1627\log 2}{42} - \frac{729\log 3}{70} + \frac{77\log y}{12} \right) \\
& + e \left\{ \cos \chi \left[-2y^3 - \frac{76}{9}\pi y^{11/2} + y^4 \left(-\frac{13}{9} - \frac{8\gamma_E}{3} - \frac{5\pi^2}{32} - \frac{40\log 2}{3} - \frac{4\log y}{3} \right) \right. \right. \\
& \quad \left. + y^5 \left(\frac{1031}{60} + 12\gamma_E - \frac{2709\pi^2}{512} + \frac{516\log 2}{5} - \frac{243\log 3}{5} - 2\log y \right) \right. \\
& \quad \left. + y^6 \left(-\frac{13035}{56} + \frac{29\gamma_E}{3} + \frac{1473\pi^2}{512} - \frac{20227\log 2}{35} + \frac{36693\log 3}{70} + \frac{341\log y}{6} \right) \right] \\
& \quad \left. + \left[-y^{5/2} + \frac{3y^{7/2}}{2} + \frac{2\pi y^4}{3} - \frac{65y^{9/2}}{24} - \frac{146\pi y^5}{15} - \frac{715\pi y^6}{84} \right. \right. \\
& \quad \left. \left. + y^{11/2} \left(\frac{354839}{3600} - \frac{76\gamma_E}{5} + 4\pi^2 - \frac{452\log 2}{9} - \frac{78\log y}{5} \right) \right] \sin \chi \right\} \\
& + e^2 \left\{ -4y^3 - \frac{646}{45}\pi y^{11/2} + y^5 \left(\frac{2933}{45} + \frac{50\gamma_E}{3} - \frac{5597\pi^2}{1024} + \frac{2494\log 2}{15} - \frac{486\log 3}{5} - \frac{11\log y}{3} \right) \right. \\
& \quad \left. + y^4 \left(\frac{101}{9} - \frac{20\gamma_E}{3} - \frac{13\pi^2}{16} - \frac{68\log 2}{3} - \frac{10\log y}{3} \right) \right. \\
& \quad \left. + y^6 \left(-\frac{266261}{840} + \frac{809\gamma_E}{6} + \frac{25323\pi^2}{2048} - \frac{10729\log 2}{10} + \frac{72657\log 3}{70} + \frac{1793\log y}{12} \right) \right. \\
& \quad \left. + \cos 2\chi \left[y^3 - \frac{1349}{90}\pi y^{11/2} + y^5 \left(\frac{2093}{120} + 38\gamma_E - \frac{21183\pi^2}{1024} - \frac{4862\log 2}{5} + \frac{14013\log 3}{20} - 9\log y \right) \right. \right. \\
& \quad \left. + y^4 \left(-\frac{151}{6} + 4\gamma_E + \frac{3\pi^2}{2} + \frac{172\log 2}{3} - \frac{81\log 3}{2} + 2\log y \right) - y^6 \left(\frac{85703}{112} \right. \right. \\
& \quad \left. \left. + \frac{1271\gamma_E}{6} - \frac{65457\pi^2}{2048} - \frac{2070871\log 2}{210} + \frac{30564\log 3}{7} + \frac{390625\log 5}{336} - \frac{1825\log y}{12} \right) \right] \\
& \quad \left. + \sin 2\chi \left[-y^{5/2} + 4y^{7/2} - \frac{11\pi y^4}{6} - \frac{283y^{9/2}}{24} - \frac{241\pi y^5}{12} + \frac{6337\pi y^6}{70} \right] \right\}
\end{aligned}$$

$$\begin{aligned}
& + y^{11/2} \left(\frac{190159}{1800} - \frac{152\gamma_E}{5} + 8\pi^2 + \frac{2192 \log 2}{45} - \frac{1539 \log 3}{10} - \frac{356 \log y}{5} \right) \Big] \Big\} \\
+ e^3 & \left\{ \cos 3\chi \left[\frac{3y^3}{2} - \frac{893}{108} \pi y^{11/2} + y^4 \left(-\frac{1231}{36} + \frac{20\gamma_E}{3} + \frac{31\pi^2}{16} - \frac{2860 \log 2}{9} + \frac{837 \log 3}{4} + \frac{10 \log y}{3} \right) \right. \right. \\
& + y^5 \left(\frac{54349}{720} + \frac{80\gamma_E}{3} - \frac{62041\pi^2}{2048} + \frac{331304 \log 2}{45} - \frac{14769 \log 3}{5} - \frac{78125 \log 5}{72} - \frac{68 \log y}{3} \right) \\
& - y^6 \left(\frac{246899}{288} + \frac{2527\gamma_E}{6} - \frac{392859\pi^2}{4096} + \frac{15316951 \log 2}{210} - \frac{53091 \log 3}{7} - \frac{52496875 \log 5}{2016} \right. \\
& \left. \left. - \frac{3689 \log y}{12} \right) \right] + \cos \chi \left[-\frac{11y^3}{2} - \frac{11989}{180} \pi y^{11/2} + y^4 \left(-\frac{649}{36} - \frac{20\gamma_E}{3} + \frac{7\pi^2}{8} + \frac{292 \log 2}{3} \right. \right. \\
& - \frac{405 \log 3}{4} - \frac{10 \log y}{3} \left. \right) + y^5 \left(\frac{156571}{720} + \frac{304\gamma_E}{3} - \frac{111599\pi^2}{2048} - \frac{38144 \log 2}{15} + \frac{14499 \log 3}{8} \right. \\
& - \frac{100 \log y}{3} \left. \right) + y^6 \left(-\frac{2511063}{1120} - \frac{1057\gamma_E}{6} + \frac{567333\pi^2}{4096} + \frac{1241395 \log 2}{42} - \frac{6311169 \log 3}{560} \right. \\
& \left. - \frac{390625 \log 5}{96} + \frac{8807 \log y}{12} \right) \Big] + \sin \chi \left[-\frac{11y^{5/2}}{4} + \frac{97y^{7/2}}{8} - \frac{5\pi y^4}{12} - \frac{565y^{9/2}}{32} - \frac{2481\pi y^5}{40} \right. \\
& \left. + \frac{39017\pi y^6}{280} + y^{11/2} \left(\frac{9289201}{14400} - \frac{551\gamma_E}{5} + 29\pi^2 + \frac{2803 \log 2}{45} - \frac{1539 \log 3}{4} - \frac{1731 \log y}{10} \right) \right] \\
& + \sin 3\chi \left[-\frac{y^{5/2}}{4} + \frac{35y^{7/2}}{8} - \frac{121\pi y^4}{36} - \frac{1621y^{9/2}}{96} - \frac{377\pi y^5}{30} + \frac{1068661\pi y^6}{5040} \right. \\
& \left. + y^{11/2} \left(-\frac{709127}{4800} - \frac{247\gamma_E}{15} + \frac{13\pi^2}{3} - \frac{23053 \log 2}{15} + \frac{15903 \log 3}{20} - \frac{3907 \log y}{30} \right) \right] \Big\} \\
+ e^4 & \left\{ -\frac{71y^3}{8} - \frac{10697}{144} \pi y^{11/2} + y^4 \left(\frac{4703}{144} - \frac{103\gamma_E}{6} - \frac{379\pi^2}{256} + \frac{329 \log 2}{6} - \frac{1377 \log 3}{16} - \frac{103 \log y}{12} \right) \right. \\
& + y^5 \left(\frac{63521}{192} + \frac{357\gamma_E}{4} - \frac{161847\pi^2}{4096} - \frac{50399 \log 2}{20} + \frac{276129 \log 3}{160} - \frac{267 \log y}{8} \right) + y^6 \left(-\frac{31438061}{13440} \right. \\
& \left. + \frac{22507\gamma_E}{48} + \frac{1452237\pi^2}{8192} + \frac{57264337 \log 2}{1680} - \frac{6320889 \log 3}{560} - \frac{14453125 \log 5}{2688} + \frac{101227 \log y}{96} \right) \\
& + \cos 4\chi \left[\frac{3y^3}{8} + \frac{2185}{864} \pi y^{11/2} + y^4 \left(-\frac{2731}{144} + \frac{19\gamma_E}{6} + \frac{223\pi^2}{256} + \frac{25961 \log 2}{18} - \frac{16119 \log 3}{32} \right. \right. \\
& - \frac{78125 \log 5}{288} + \frac{19 \log y}{12} \left. \right) + y^5 \left(\frac{50149}{320} - \frac{73\gamma_E}{4} - \frac{93345\pi^2}{4096} - \frac{6150733 \log 2}{180} + \frac{1172799 \log 3}{320} \right. \\
& \left. + \frac{7035625 \log 5}{576} - \frac{249 \log y}{8} \right) + y^6 \left(-\frac{12447469}{40320} - \frac{15047\gamma_E}{48} + \frac{1135995\pi^2}{8192} + \frac{363730429 \log 2}{1008} \right. \\
& \left. + \frac{49057083 \log 3}{560} - \frac{749322125 \log 5}{4032} - \frac{282475249 \log 7}{11520} + \frac{39289 \log y}{96} \right) \Big] \\
& + \cos 2\chi \left[\frac{7y^3}{2} - \frac{15637}{180} \pi y^{11/2} + y^4 \left(-\frac{4867}{36} + \frac{62\gamma_E}{3} + \frac{469\pi^2}{64} - \frac{8950 \log 2}{9} + \frac{2511 \log 3}{4} + \frac{31 \log y}{3} \right) \right. \\
& + y^5 \left(\frac{75947}{240} + 171\gamma_E - \frac{37323\pi^2}{256} + \frac{1171843 \log 2}{45} - \frac{380781 \log 3}{40} - \frac{78125 \log 5}{18} - \frac{189 \log y}{2} \right) \\
& + y^6 \left(-\frac{6413707}{1440} - \frac{26419\gamma_E}{12} + \frac{251931\pi^2}{512} - \frac{50395357 \log 2}{180} + \frac{5054157 \log 3}{280} + \frac{72521875 \log 5}{672} \right. \\
& \left. + \frac{33917 \log y}{24} \right) \Big] + \sin 2\chi \left[-\frac{5y^{5/2}}{2} + \frac{83y^{7/2}}{4} - \frac{353\pi y^4}{36} - \frac{3601y^{9/2}}{48} - \frac{11191\pi y^5}{120} + \frac{24571\pi y^6}{24} \right. \\
& \left. + y^{11/2} \left(\frac{547051}{1440} - \frac{532\gamma_E}{3} + \frac{140\pi^2}{3} - \frac{47080 \log 2}{9} + \frac{47709 \log 3}{20} - \frac{1646 \log y}{3} \right) \right] \Big\}
\end{aligned}$$

$$\begin{aligned}
& + \sin 4\chi \left[\frac{17y^{7/2}}{8} - \frac{457\pi y^4}{288} - \frac{611y^{9/2}}{48} + \frac{8491\pi y^5}{960} + \frac{851239\pi y^6}{5376} + y^{11/2} \left(-\frac{4896077}{14400} \right. \right. \\
& \left. \left. + \frac{76\gamma_E}{15} - \frac{4\pi^2}{3} + \frac{923608 \log 2}{135} - \frac{306261 \log 3}{160} - \frac{1484375 \log 5}{864} - \frac{1822 \log y}{15} \right) \right] \Bigg\}, \quad (3.21)
\end{aligned}$$

where γ_E is the Euler-Mascheroni constant, and the result reduces to the circular case in the limit $e \rightarrow 0$. In Fig. 1, we show the impact of the eccentricity with respect to y for different values of e and different angular configurations, i.e. $\chi = 0, \pi, 2\pi$. By carefully looking at Eq. (3.21), it is clear that the only χ -dependence of the field is through trigonometric functions, that reflect the periodic motion of the source. This is also shown in the aforementioned plot, where the two lines for $\chi = 0$ and 2π are completely overlapping.

In the next Section, we will use the results found above to compute the Self-Force components.

IV. SCALAR SELF-FORCE

We recall that the unit-mass SSF acting on a scalar charge is given by

$$F_\alpha(t) = \frac{q}{\mu} P_\alpha^\beta(t) \nabla_\beta \psi_R, \quad (4.1)$$

where ψ_R is the regularized field (discussed in the previous Section) evaluated at the particle position and $P_\alpha^\beta(t) = \delta_\alpha^\beta + u_\alpha u^\beta$ projects orthogonally to the particle's world-line. It is important to point out that the scalar force scales as $F_\alpha(t) \propto q^2/\mu M^2$, or alternatively $F_\alpha(t) = O(\varepsilon/M)$. By considering this force small, we are

indeed asking that

$$\varepsilon = \frac{q^2}{\mu M} \ll 1. \quad (4.2)$$

These considerations will be important in later stages of this paper (Sec. VI), where we will compare our results with independent computations performed in scalar-tensor theories with the post-Newtonian formalism.

Since we are restricting the motion to the equatorial plane, there are three non-vanishing components of the self-force which take the following form

$$\begin{aligned}
F_t(t) &= \frac{q}{\mu} (1 - u_t^2 f(r_p(t))) \partial_t \psi_R \\
&\quad - \frac{q}{\mu} f(r_p(t)) u_t (u_r \partial_r \psi_R + u_\phi \partial_\phi \psi_R), \quad (4.3)
\end{aligned}$$

$$\begin{aligned}
F_r(t) &= \frac{q}{\mu} (1 + u_r^2 f^{-1}(r_p(t))) \partial_r \psi_R \\
&\quad + \frac{q}{\mu} u_r f^{-1}(r_p(t)) (u_t \partial_t \psi_R + u_\phi \partial_\phi \psi_R), \quad (4.4)
\end{aligned}$$

$$\begin{aligned}
F_\phi(t) &= \frac{q}{\mu} (1 + r_p^2(t) u_\phi^2) \partial_\phi \psi_R \\
&\quad + \frac{q}{\mu} u_\phi r_p^2(t) (u_t \partial_t \psi_R + u_r \partial_r \psi_R). \quad (4.5)
\end{aligned}$$

In analogy with the calculations performed in the previous Section, in order to construct the derivative of the regularized scalar field, we first have to compute the same derivatives for the retarded field, i.e.

$$\partial_t \psi^{\text{ret}}(t) = \sum_{lm} \partial_t (e^{-im\Omega_\phi t} \bar{\psi}_{lm}(t, r)) Y_{lm}(\theta, \phi) \Big|_{(r, \theta, \phi) \rightarrow (r_p(t), \pi/2, \phi_p(t))}, \quad (4.6)$$

$$\partial_r \psi^{\text{ret}}(t) = \sum_{lm} e^{-im\Omega_\phi t} \partial_r \bar{\psi}_{lm}(t, r) Y_{lm}(\theta, \phi) \Big|_{(r, \theta, \phi) \rightarrow (r_p(t), \pi/2, \phi_p(t))}, \quad (4.7)$$

$$\partial_\phi \psi^{\text{ret}}(t) = \sum_{lm} (im) e^{-im\Omega_\phi t} \bar{\psi}_{lm}(t, r) Y_{lm}(\theta, \phi) \Big|_{(r, \theta, \phi) \rightarrow (r_p(t), \pi/2, \phi_p(t))}, \quad (4.8)$$

which needs to be regularized. Alternatively, we can directly compute the non-regularized components of the force with the derivatives of the scalar field and then use the mode-sum regularization directly on the forces. For

our purposes, we will follow the first methodology but we checked that the two methods are indeed equivalent.

Accordingly, the regularized self-force is obtained by subtracting the divergent term $B_\alpha(t)$ after performing

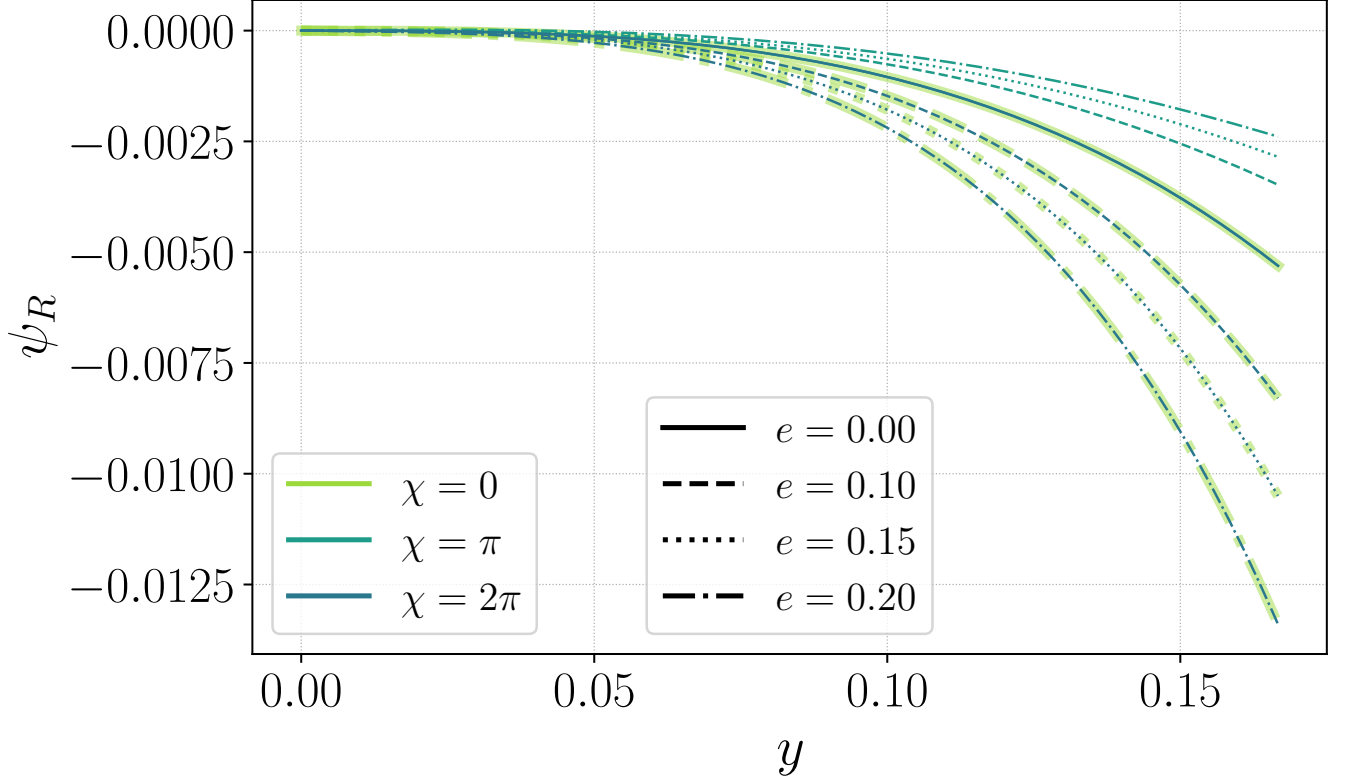


FIG. 1: Regularized field $\psi_R(y, e; \chi)$ evaluated at $\chi = 0, \pi, 2\pi$, setting $M = 1$.

the m -mode summation and evaluating at the particle's position as follows

$$F_\alpha^R(t) = \sum_l \left\{ \frac{1}{2} \left(F_{\alpha(+)}^l(t) - F_{\alpha(-)}^l(t) \right) - B_\alpha(t) \right\}, \quad (4.9)$$

where the \pm is used to show that we are evaluating the l -modes of the force components at the particle position $r \rightarrow r_p^\pm(t)$.

By using the same convention as before, the subtraction terms are (in units of ε) as functions of χ

$$\begin{aligned}
B_t(y, e; \chi) &= e \sin \chi \left(\frac{y^{5/2}}{2} - \frac{5y^{7/2}}{8} - \frac{375y^{9/2}}{128} - \frac{6181y^{11/2}}{512} \right) + e^2 \sin 2\chi \left(\frac{y^{5/2}}{2} - \frac{y^{7/2}}{2} - \frac{749y^{9/2}}{128} - \frac{5531y^{11/2}}{256} \right) \\
&+ e^3 \left[\left(\frac{11y^{5/2}}{8} - \frac{33y^{7/2}}{8} - \frac{10983y^{9/2}}{512} - \frac{75889y^{11/2}}{1024} \right) \sin \chi + \left(\frac{y^{5/2}}{8} + \frac{y^{7/2}}{16} - \frac{2761y^{9/2}}{512} - \frac{6933y^{11/2}}{512} \right) \sin 3\chi \right] \\
&+ e^4 \left[\left(\frac{5y^{5/2}}{4} - \frac{7y^{7/2}}{2} - \frac{9131y^{9/2}}{256} - \frac{24751y^{11/2}}{256} \right) \sin 2\chi + \left(\frac{y^{7/2}}{8} - \frac{779y^{9/2}}{256} - \frac{845y^{11/2}}{1024} \right) \sin 4\chi \right], \quad (4.10a) \\
B_r(y, e; \chi) &= -\frac{y^2}{2} - \frac{y^3}{8} - \frac{21y^4}{128} - \frac{53y^5}{512} + \frac{12607y^6}{32768} + e \cos \chi \left(-y^2 - \frac{y^3}{2} - \frac{15y^4}{64} + \frac{73y^5}{64} + \frac{93563y^6}{16384} \right) \\
&+ e^2 \left[-\frac{5y^2}{4} + y^3 + \frac{1661y^4}{256} + \frac{16547y^5}{512} + \frac{10397703y^6}{65536} + \cos 2\chi \left(-\frac{y^2}{4} - \frac{y^3}{8} + \frac{101y^4}{256} - \frac{13y^5}{64} - \frac{475373y^6}{65536} \right) \right] \\
&+ e^3 \left[\cos \chi \left(-2y^2 + \frac{15y^3}{8} + \frac{1981y^4}{128} + \frac{4739y^5}{64} + \frac{5584373y^6}{16384} \right) + \cos 3\chi \left(\frac{y^3}{8} + \frac{103y^4}{128} - \frac{179y^5}{64} - \frac{396111y^6}{16384} \right) \right]
\end{aligned}$$

$$\begin{aligned}
& + e^4 \left[-2y^2 + \frac{273y^3}{64} + \frac{27663y^4}{1024} + \frac{269205y^5}{2048} + \frac{83361301y^6}{131072} \right. \\
& \quad \left. - \cos 2\chi \left(\frac{y^2}{2} - \frac{9y^3}{16} - \frac{1689y^4}{256} - \frac{6273y^5}{512} - \frac{34369y^6}{2048} \right) + \cos 4\chi \left(\frac{3y^3}{64} + \frac{581y^4}{1024} - \frac{6157y^5}{2048} - \frac{2618153y^6}{131072} \right) \right], \tag{4.10b}
\end{aligned}$$

$$\begin{aligned}
B_\phi(y, e; \chi) &= e \sin \chi \left(-\frac{3y^2}{4} + \frac{15y^3}{32} + \frac{1119y^4}{256} + \frac{83079y^5}{4096} + \frac{5078371y^6}{65536} \right) \\
& + e^2 \left(-\frac{3y^2}{4} + \frac{21y^3}{16} + \frac{1785y^4}{256} + \frac{29217y^5}{1024} + \frac{8221319y^6}{65536} \right) \sin 2\chi \\
& + e^3 \left[\sin \chi \left(-\frac{27y^2}{16} + \frac{303y^3}{64} + \frac{26265y^4}{1024} + \frac{108537y^5}{1024} + \frac{127678143y^6}{262144} \right) \right. \\
& \quad \left. + \sin 3\chi \left(-\frac{3y^2}{16} + \frac{69y^3}{64} + \frac{3369y^4}{1024} + \frac{44913y^5}{4096} + \frac{15633911y^6}{262144} \right) \right] \\
& + e^4 \left[\sin 2\chi \left(-\frac{3y^2}{2} + \frac{219y^3}{32} + \frac{7419y^4}{256} + \frac{214545y^5}{2048} + \frac{8669885y^6}{16384} \right) \right. \\
& \quad \left. + \sin 4\chi \left(\frac{21y^3}{64} - \frac{9y^4}{512} - \frac{3249y^5}{4096} - \frac{534939y^6}{65536} \right) \right]. \tag{4.10c}
\end{aligned}$$

We can ultimately show the final result for the three SSF components, reading as

$$\begin{aligned}
F_t(y, e; \chi) &= \frac{y^4}{3} - \frac{y^5}{6} + \frac{2}{3}\pi y^{11/2} - \frac{77y^6}{24} + e \left\{ \left(\frac{5y^4}{3} - \frac{5y^5}{2} + 6\pi y^{11/2} - \frac{653y^6}{24} \right) \cos \chi \right. \\
& \quad \left. + \left[2y^{9/2} + y^{11/2} \left(-\frac{187}{9} + \frac{28\gamma_E}{3} + \frac{35\pi^2}{64} + 20 \log 2 + \frac{14 \log y}{3} \right) \right] \sin \chi \right\} \\
& + e^2 \left\{ \frac{8y^4}{3} - \frac{13y^5}{6} + \frac{32}{3}\pi y^{11/2} - \frac{299y^6}{4} + \cos 2\chi \left(2y^4 - \frac{23y^5}{2} + \frac{89}{6}\pi y^{11/2} - \frac{91y^6}{2} \right) \right. \\
& \quad \left. + \sin 2\chi \left[5y^{9/2} + y^{11/2} \left(-\frac{1343}{18} + \frac{88\gamma_E}{3} + \frac{119\pi^2}{64} + \frac{56 \log 2}{3} + \frac{81 \log 3}{2} + \frac{44 \log y}{3} \right) \right] \right\} \\
& + e^3 \left\{ \cos \chi \left(\frac{26y^4}{3} - \frac{82y^5}{3} + \frac{331}{6}\pi y^{11/2} - \frac{1245y^6}{4} \right) + \cos 3\chi \left(\frac{4y^4}{3} - \frac{53y^5}{3} + \frac{181}{9}\pi y^{11/2} - \frac{152y^6}{3} \right) \right. \\
& \quad + \sin \chi \left[14y^{9/2} + y^{11/2} \left(-\frac{4105}{18} + \frac{251\gamma_E}{3} + \frac{1309\pi^2}{256} + \frac{139 \log 2}{3} + \frac{243 \log 3}{2} + \frac{251 \log y}{6} \right) \right] \\
& \quad \left. + \sin 3\chi \left[5y^{9/2} + y^{11/2} \left(-\frac{1051}{9} + \frac{121\gamma_E}{3} + \frac{707\pi^2}{256} + 275 \log 2 - 81 \log 3 + \frac{121 \log y}{6} \right) \right] \right\} + \\
& + e^4 \left\{ \frac{217y^4}{24} - \frac{275y^5}{16} + \frac{2831}{48}\pi y^{11/2} - \frac{31703y^6}{64} + \cos 2\chi \left(\frac{53y^4}{6} - \frac{333y^5}{4} + \frac{3781}{36}\pi y^{11/2} - \frac{15301y^6}{48} \right) \right. \\
& \quad + \cos 4\chi \left(\frac{11y^4}{24} - \frac{193y^5}{16} + \frac{4421}{288}\pi y^{11/2} - \frac{9823y^6}{192} \right) \\
& \quad + \sin 2\chi \left[\frac{55y^{9/2}}{2} + y^{11/2} \left(-\frac{2483}{4} + \frac{620\gamma_E}{3} + \frac{1715\pi^2}{128} + \frac{10180 \log 2}{9} - \frac{1053 \log 3}{4} + \frac{310 \log y}{3} \right) \right] \\
& \quad \left. + \sin 4\chi \left[\frac{5y^{9/2}}{2} - y^{11/2} \left(\frac{895}{9} - \frac{92\gamma_E}{3} - \frac{287\pi^2}{128} + \frac{1964 \log 2}{3} - \frac{3321 \log 3}{32} - \frac{78125 \log 5}{288} - \frac{46 \log y}{3} \right) \right] \right\}, \tag{4.11a}
\end{aligned}$$

$$F_r(y, e; \chi) = y^5 \left(-\frac{2}{9} - \frac{4\gamma_E}{3} + \frac{7\pi^2}{64} - \frac{4 \log 2}{3} - \frac{2 \log y}{3} \right) + y^6 \left(\frac{604}{45} - \frac{14\gamma_E}{3} + \frac{29\pi^2}{1024} - \frac{66 \log 2}{5} - \frac{7 \log y}{3} \right)$$

$$\begin{aligned}
& + e \left\{ \cos \chi \left[y^5 \left(\frac{92}{9} - \frac{32\gamma_E}{3} + \frac{7\pi^2}{32} - \frac{64 \log 2}{3} - \frac{16 \log y}{3} \right) \right. \right. \\
& \quad \left. \left. + y^6 \left(\frac{3694}{45} - \frac{8\gamma_E}{3} + \frac{565\pi^2}{128} + \frac{512 \log 2}{5} - \frac{486 \log 3}{5} + \frac{20 \log y}{3} \right) \right] \right. \\
& \quad \left. + \sin \chi \left(\frac{2y^{7/2}}{3} - 8y^{9/2} + 4\pi y^5 - \frac{61y^{11/2}}{4} - \frac{154\pi y^6}{15} \right) \right\} \\
& + e^2 \left\{ y^5 \left(\frac{136}{9} - \frac{58\gamma_E}{3} + \frac{77\pi^2}{128} - \frac{122 \log 2}{3} - \frac{29 \log y}{3} \right) \right. \\
& \quad + y^6 \left(\frac{10136}{45} - \frac{67\gamma_E}{3} + \frac{1543\pi^2}{256} + \frac{653 \log 2}{3} - 243 \log 3 + \frac{29 \log y}{6} \right) \\
& \quad + \cos 2\chi \left[y^5 \left(\frac{368}{9} - \frac{62\gamma_E}{3} - \frac{77\pi^2}{128} + \frac{2 \log 2}{3} - \frac{81 \log 3}{2} - \frac{31 \log y}{3} \right) \right. \\
& \quad \left. + y^6 \left(\frac{4142}{45} + \frac{227\gamma_E}{3} + \frac{8543\pi^2}{512} - 1247 \log 2 + \frac{17577 \log 3}{20} + \frac{419 \log y}{6} \right) \right] \\
& \quad \left. + \sin 2\chi \left(y^{7/2} - \frac{44y^{9/2}}{3} + \frac{61\pi y^5}{6} - \frac{1357y^{11/2}}{24} - \frac{2641\pi y^6}{60} \right) \right\} \\
& + e^3 \left\{ \cos 3\chi \left[y^5 \left(\frac{991}{18} - \frac{64\gamma_E}{3} - \frac{77\pi^2}{64} - \frac{2512 \log 2}{9} + \frac{243 \log 3}{2} - \frac{32 \log y}{3} \right) \right. \right. \\
& \quad \left. \left. + y^6 \left(\frac{3679}{36} + \frac{418\gamma_E}{3} + \frac{11347\pi^2}{512} + \frac{442168 \log 2}{45} - \frac{54351 \log 3}{20} - \frac{78125 \log 5}{36} + \frac{359 \log y}{3} \right) \right] \right. \\
& \quad + \cos \chi \left[y^5 \left(\frac{2213}{18} - \frac{256\gamma_E}{3} + \frac{7\pi^2}{64} - 48 \log 2 - \frac{243 \log 3}{2} - \frac{128 \log y}{3} \right) \right. \\
& \quad \left. + y^6 \left(\frac{14753}{20} + 154\gamma_E + \frac{27057\pi^2}{512} - \frac{60448 \log 2}{15} + \frac{25353 \log 3}{10} + 195 \log y \right) \right] \\
& \quad + \sin \chi \left(\frac{17y^{7/2}}{6} - \frac{201y^{9/2}}{4} + \frac{181\pi y^5}{6} - \frac{5257y^{11/2}}{48} - \frac{4513\pi y^6}{30} \right) \\
& \quad \left. + \sin 3\chi \left(\frac{y^{7/2}}{2} - \frac{37y^{9/2}}{4} + \frac{193\pi y^5}{18} - \frac{1429y^{11/2}}{16} - \frac{4157\pi y^6}{60} \right) \right\} \\
& + e^4 \left\{ y^5 \left(\frac{8363}{72} - \frac{569\gamma_E}{6} + \frac{707\pi^2}{512} - \frac{313 \log 2}{6} - \frac{2187 \log 3}{16} - \frac{569 \log y}{12} \right) \right. \\
& \quad + y^6 \left(\frac{96289}{80} + \frac{323\gamma_E}{4} + \frac{199149\pi^2}{4096} - \frac{332851 \log 2}{60} + \frac{517347 \log 3}{160} + \frac{1411 \log y}{8} \right) \\
& \quad + \cos 4\chi \left[y^5 \left(\frac{2425}{72} - \frac{71\gamma_E}{6} - \frac{427\pi^2}{512} + \frac{16811 \log 2}{18} - \frac{7371 \log 3}{32} - \frac{78125 \log 5}{288} - \frac{71 \log y}{12} \right) \right. \\
& \quad \left. + y^6 \left(\frac{25087}{144} + \frac{373\gamma_E}{4} + \frac{48147\pi^2}{4096} - \frac{817943 \log 2}{20} - \frac{84969 \log 3}{64} + \frac{10785625 \log 5}{576} + \frac{693 \log y}{8} \right) \right] \\
& \quad + \cos 2\chi \left[y^5 \left(\frac{1711}{6} - \frac{380\gamma_E}{3} - \frac{35\pi^2}{8} - \frac{10036 \log 2}{9} + 405 \log 3 - \frac{190 \log y}{3} \right) \right. \\
& \quad \left. + y^6 \left(\frac{76943}{180} + 776\gamma_E + \frac{135639\pi^2}{1024} + \frac{1797784 \log 2}{45} - \frac{379323 \log 3}{40} - \frac{78125 \log 5}{8} + 660 \log y \right) \right] \\
& \quad + \sin 2\chi \left(\frac{11y^{7/2}}{3} - \frac{309y^{9/2}}{4} + \frac{185\pi y^5}{3} - \frac{4051y^{11/2}}{12} - \frac{52057\pi y^6}{120} \right) \\
& \quad \left. + \sin 4\chi \left(\frac{y^{7/2}}{12} - \frac{15y^{9/2}}{8} + \frac{1699\pi y^5}{288} - \frac{2519y^{11/2}}{32} - \frac{44617\pi y^6}{960} \right) \right\}, \tag{4.11b}
\end{aligned}$$

$$\begin{aligned}
F_\phi(y, e; \chi) = & -\frac{y^{5/2}}{3} + \frac{y^{7/2}}{6} - \frac{2\pi y^4}{3} + \frac{77y^{9/2}}{24} - \frac{9\pi y^5}{5} + \frac{601\pi y^6}{84} - y^{11/2} \left(\frac{10121}{3600} - \frac{76\gamma_E}{45} + \frac{4\pi^2}{9} - \frac{76 \log 2}{45} - \frac{38 \log y}{45} \right) \\
& + e \left\{ \cos \chi \left[-y^{5/2} + \frac{3y^{7/2}}{2} - \frac{14\pi y^4}{3} + \frac{475y^{9/2}}{24} + \frac{21\pi y^5}{5} + \frac{53167\pi y^6}{420} \right. \right. \\
& \quad \left. \left. + y^{11/2} \left(-\frac{98161}{720} + \frac{76\gamma_E}{3} - \frac{20\pi^2}{3} + \frac{2356 \log 2}{45} + \frac{38 \log y}{3} \right) \right] \right. \\
& \quad + \sin \chi \left[-2y^3 - \frac{532}{45}\pi y^{11/2} + y^4 \left(21 - 8\gamma_E - \frac{21\pi^2}{32} - \frac{56 \log 2}{3} - 4 \log y \right) \right. \\
& \quad \left. + y^5 \left(\frac{7981}{180} + \frac{76\gamma_E}{3} + \frac{773\pi^2}{256} + \frac{804 \log 2}{5} - \frac{486 \log 3}{5} + \frac{38 \log y}{3} \right) \right. \\
& \quad \left. \left. + y^6 \left(-\frac{10565}{24} + \frac{929\gamma_E}{3} + \frac{2193\pi^2}{1024} - \frac{31723 \log 2}{35} + \frac{7533 \log 3}{7} + \frac{929 \log y}{6} \right) \right] \right\} \\
& + e^2 \left\{ -\frac{4y^{5/2}}{3} + \frac{8y^{7/2}}{3} - \frac{20\pi y^4}{3} + \frac{127y^{9/2}}{3} - \frac{44\pi y^5}{15} + \frac{16279\pi y^6}{70} \right. \\
& \quad + y^{11/2} \left(-\frac{142763}{900} + \frac{1672\gamma_E}{45} - \frac{88\pi^2}{9} + \frac{3496 \log 2}{45} + \frac{836 \log y}{45} \right) \\
& \quad + \cos 2\chi \left[-\frac{y^{5/2}}{2} + \frac{13y^{7/2}}{4} - \frac{47\pi y^4}{6} + \frac{1223y^{9/2}}{48} + \frac{157\pi y^5}{4} + \frac{13879\pi y^6}{30} \right. \\
& \quad \left. + y^{11/2} \left(-\frac{942211}{1440} + \frac{266\gamma_E}{3} - \frac{70\pi^2}{3} + \frac{190 \log 2}{9} + \frac{1539 \log 3}{10} + \frac{133 \log y}{3} \right) \right] \\
& \quad + \sin 2\chi \left[-3y^3 - \frac{4009}{90}\pi y^{11/2} + y^4 \left(\frac{93}{2} - 16\gamma_E - \frac{21\pi^2}{16} + \frac{32 \log 2}{3} - \frac{81 \log 3}{2} - 8 \log y \right) \right. \\
& \quad \left. + y^5 \left(\frac{24539}{360} + \frac{244\gamma_E}{3} + \frac{1715\pi^2}{256} - \frac{20612 \log 2}{15} + \frac{19521 \log 3}{20} + \frac{122 \log y}{3} \right) \right. \\
& \quad \left. - y^6 \left(\frac{10832999}{5040} - \frac{2998\gamma_E}{3} + \frac{3655\pi^2}{256} - \frac{429400 \log 2}{21} + \frac{1521369 \log 3}{280} + \frac{390625 \log 5}{112} \right. \right. \\
& \quad \left. \left. - \frac{1511 \log y}{3} \right) \right] \right\} \\
& + e^3 \left\{ \cos 3\chi \left[-\frac{y^{5/2}}{12} + \frac{73y^{7/2}}{24} - \frac{217\pi y^4}{36} + \frac{1829y^{9/2}}{96} + \frac{4381\pi y^5}{72} + \frac{162293\pi y^6}{240} \right. \right. \\
& \quad \left. \left. + y^{11/2} \left(-\frac{10109743}{8640} + \frac{1273\gamma_E}{9} - \frac{335\pi^2}{9} + \frac{189031 \log 2}{135} - \frac{10773 \log 3}{20} + \frac{1273 \log y}{18} \right) \right] \right. \\
& \quad + \cos \chi \left[-\frac{11y^{5/2}}{4} + \frac{87y^{7/2}}{8} - \frac{319\pi y^4}{12} + \frac{4575y^{9/2}}{32} + \frac{655\pi y^5}{8} + \frac{916021\pi y^6}{560} \right. \\
& \quad \left. + y^{11/2} \left(-\frac{4967561}{2880} + \frac{779\gamma_E}{3} - \frac{205\pi^2}{3} + \frac{5909 \log 2}{45} + \frac{1539 \log 3}{4} + \frac{779 \log y}{6} \right) \right] \\
& \quad + \sin \chi \left[-\frac{15y^3}{2} - \frac{21109}{180}\pi y^{11/2} + y^4 \left(\frac{557}{4} - 44\gamma_E - \frac{231\pi^2}{64} + \frac{52 \log 2}{3} - \frac{405 \log 3}{4} - 22 \log y \right) \right. \\
& \quad \left. + y^5 \left(\frac{41569}{240} + 250\gamma_E + \frac{25407\pi^2}{1024} - \frac{58534 \log 2}{15} + \frac{109431 \log 3}{40} + 125 \log y \right) \right. \\
& \quad \left. + y^6 \left(-\frac{68619637}{10080} + \frac{9892\gamma_E}{3} - \frac{34931\pi^2}{2048} + \frac{1366471 \log 2}{21} - \frac{2215809 \log 3}{140} - \frac{390625 \log 5}{32} \right. \right. \\
& \quad \left. \left. + \frac{4946 \log y}{3} \right) \right] + \sin 3\chi \left[-\frac{3y^3}{2} - \frac{38171}{540}\pi y^{11/2} + y^4 \left(\frac{475}{12} - 12\gamma_E - \frac{63\pi^2}{64} \right) \right.
\end{aligned}$$

$$\begin{aligned}
& - \frac{844 \log 2}{3} + \frac{567 \log 3}{4} - 6 \log y \Big) + y^5 \left(- \frac{22409}{720} + \frac{358 \gamma_E}{3} + \frac{5435 \pi^2}{1024} + \frac{96046 \log 2}{9} \right. \\
& - \frac{131463 \log 3}{40} - \frac{78125 \log 5}{36} + \frac{179 \log y}{3} \Big) + y^6 \left(- \frac{1197899}{288} + \frac{4030 \gamma_E}{3} \right. \\
& \left. - \frac{130115 \pi^2}{2048} - \frac{38386721 \log 2}{315} - \frac{20439 \log 3}{7} + \frac{115853125 \log 5}{2016} + \frac{2063 \log y}{3} \right) \Big] \Big\} \\
& + e^4 \left\{ - \frac{65 y^{5/2}}{24} + \frac{509 y^{7/2}}{48} - \frac{391 \pi y^4}{16} + \frac{11571 y^{9/2}}{64} + \frac{18253 \pi y^5}{480} + \frac{3933581 \pi y^6}{2240} \right. \\
& + y^{11/2} \left(- \frac{13525403}{9600} + \frac{10393 \gamma_E}{45} - \frac{547 \pi^2}{9} + 133 \log 2 + \frac{26163 \log 3}{80} + \frac{10393 \log y}{90} \right) \\
& + \cos 4\chi \left[\frac{5 y^{7/2}}{4} - \frac{577 \pi y^4}{288} + \frac{233 y^{9/2}}{24} + \frac{15641 \pi y^5}{320} + \frac{7160983 \pi y^6}{16128} \right. \\
& + y^{11/2} \left(- \frac{100663}{96} + \frac{703 \gamma_E}{6} - \frac{185 \pi^2}{6} - \frac{1405373 \log 2}{270} + \frac{180063 \log 3}{160} + \frac{1484375 \log 5}{864} \right. \\
& \left. \left. + \frac{703 \log y}{12} \right) \right] \\
& + \cos 2\chi \left[- \frac{5 y^{5/2}}{4} + \frac{117 y^{7/2}}{8} - \frac{1267 \pi y^4}{36} + \frac{12683 y^{9/2}}{96} + \frac{11709 \pi y^5}{40} + \frac{3779731 \pi y^6}{1008} \right. \\
& + y^{11/2} \left(- \frac{15245411}{2880} + \frac{1957 \gamma_E}{3} - \frac{515 \pi^2}{3} + \frac{44479 \log 2}{9} - \frac{32319 \log 3}{20} + \frac{1957 \log y}{6} \right) \Big] \\
& + \sin 2\chi \left[- \frac{19 y^3}{2} - \frac{177289}{540} \pi y^{11/2} + y^4 \left(\frac{2939}{12} - 72 \gamma_E - \frac{189 \pi^2}{32} - \frac{2912 \log 2}{3} + \frac{1701 \log 3}{4} - 36 \log y \right) \right. \\
& + y^5 \left(- \frac{4769}{720} + 612 \gamma_E + \frac{2889 \pi^2}{64} + \frac{349616 \log 2}{9} - \frac{424683 \log 3}{40} - \frac{78125 \log 5}{9} + 306 \log y \right) \\
& + y^6 \left(- \frac{43254473}{2016} + 7974 \gamma_E - \frac{219923 \pi^2}{1024} - \frac{4260481 \log 2}{9} - \frac{857007 \log 3}{28} + \frac{161528125 \log 5}{672} \right. \\
& \left. \left. + 4021 \log y \right) \right] \\
& + \sin 4\chi \left[- \frac{y^3}{4} - \frac{253061 \pi y^{11/2}}{4320} + y^4 \left(\frac{377}{24} - 4 \gamma_E - \frac{21 \pi^2}{64} + \frac{9656 \log 2}{9} - \frac{9477 \log 3}{32} \right. \right. \\
& - \frac{78125 \log 5}{288} - 2 \log y \Big) + y^5 \left(- \frac{176371}{1440} + \frac{296 \gamma_E}{3} + \frac{725 \pi^2}{512} - \frac{2057038 \log 2}{45} + \frac{34101 \log 3}{320} \right. \\
& + \frac{11410625 \log 5}{576} + \frac{148 \log y}{3} \Big) + y^6 \left(- \frac{79561903}{20160} + 882 \gamma_E - \frac{207065 \pi^2}{2048} + \frac{128020547 \log 2}{210} \right. \\
& \left. \left. + \frac{1068831207 \log 3}{4480} - \frac{1345738375 \log 5}{4032} - \frac{282475249 \log 7}{3840} + 466 \log y \right) \right] \Big\}. \tag{4.11c}
\end{aligned}$$

In analogy with the field, we show the ϕ -component of the SF and its difference with respect to the circular case in Figure 2.

Further, it is important to mention that the forces contain both conservative and dissipative contributions. In the next Sections we will focus on the dissipative sector by directly computing the fluxes.

V. SCALAR RADIATION

In this Section, the amount of scalar radiation emitted to infinity is computed by averaging over an orbital cycle. To this end, the asymptotic solutions of Eq. (3.8) are constructed by imposing the appropriate boundary conditions, namely, ingoing waves at the horizon and purely outgoing waves at infinity. A complete derivation of the energy flux at infinity is provided below. For a more

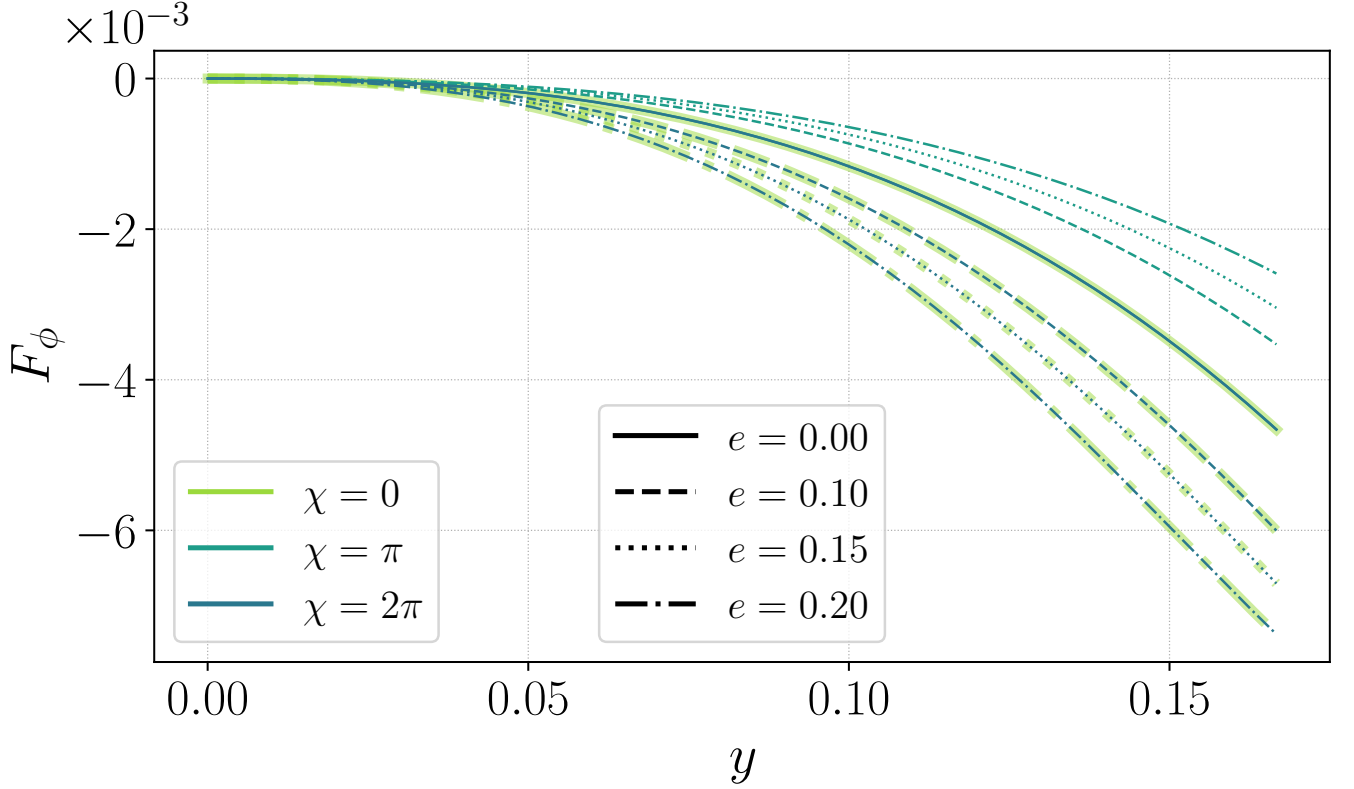


FIG. 2: Here, we show the ϕ -component of the SF. We selected the same value for both χ and e . The behaviour is rather similar to the one presented by the regularized field.

general treatment, including electromagnetic and gravitational perturbations we refer the interested reader to the original papers by Teukolsky [71–73].

The starting point is to organize the solution of the KG equation in Eq. (3.10) as

$$\psi_{lmn}(r) = -4\pi \left\{ C_{lmn}^{\text{in}}(r) R_{lmn}^{\text{in}}(r) + C_{lmn}^{\text{up}}(r) R_{lmn}^{\text{up}}(r) \right\}, \quad (5.1)$$

where

$$C_{lmn}^{\text{in}}(r) = \int_r^\infty dr' \frac{R_{lmn}^{\text{up}}(r')}{W_{lmn}} r'^2 \rho_{lmn}(r'), \quad (5.2)$$

$$C_{lmn}^{\text{up}}(r) = \int_{2M}^r dr' \frac{R_{lmn}^{\text{in}}(r')}{W_{lmn}} r'^2 \rho_{lmn}(r'). \quad (5.3)$$

Taking the limit $r \rightarrow \infty$, we notice that $C_{lmn}^{\text{in}} = 0$ and only $C_{lmn}^{\text{up}}(r)$ needs to be evaluated. Hence, the asymptotic solution takes the simplified form

$$\psi_{lmn}(r \rightarrow \infty) = -4\pi \tilde{R}_{lmn}^{\text{up}} \int_{2M}^\infty dr' \frac{R_{lmn}^{\text{in}}(r')}{W_{lmn}} r'^2 \rho_{lmn}(r'), \quad (5.4)$$

where $\tilde{R}_{lmn}^{\text{up}}$ is

$$\tilde{R}_{lmn}^{\text{up}} = C^{\text{trans}} \frac{e^{i\omega r_*}}{r}, \quad (5.5)$$

and r_* is the usual tortoise coordinate defined as

$$r_* = r + 2GM \log \left| \frac{r}{2GM} - 1 \right|. \quad (5.6)$$

Further, C^{trans} is the transmission coefficient. The latter can be computed using the MST formalism, which automatically fulfills the boundary condition we are interested in. A detailed discussion on how to compute these coefficients can be found in [69] and its expression for a scalar charge can be found in Eq. (5.10) in [74].

By using standard notation given, for instance, in [46, 69], we re-write the asymptotic field as

$$\psi_{lmn}(r \rightarrow \infty) = -4\pi e^{i\omega r_*} \frac{Z_{lmn}^\infty}{r}, \quad (5.7)$$

and its time domain counterpart can be written simply as

$$\psi_{lm}(t, r \rightarrow \infty) = -4\pi \sum_n e^{-i\omega t} e^{i\omega r_*} \frac{Z_{lmn}^\infty}{r}, \quad (5.8)$$

where the Z_{lmn}^∞ are the frequency domain amplitudes defined as

$$Z_{lmn}^\infty = C^{\text{trans}} \int_{2M}^\infty dr' \frac{R_{lmn}^{\text{in}}(r')}{W_{lmn}} r'^2 \rho_{lmn}(r'). \quad (5.9)$$

We can now directly define the outgoing energy flux. The simplest procedure that one can use is the same as

that used in [75], but here we are generalizing their discussion to the eccentric case. Let us start from the definition of the energy-momentum tensor

$$T_{\mu\nu} = \frac{\mu^2}{8\pi} \left\{ \partial_\mu \psi \partial_\nu \psi^* + \partial_\nu \psi \partial_\mu \psi^* - g_{\mu\nu} \partial^\lambda \psi \partial_\lambda \psi^* \right\}, \quad (5.10)$$

where ψ is a time domain complex scalar field and the superscript $*$ labels the complex conjugate. The energy per unit volume is then defined as

$$\frac{d^2 E^\infty}{d\Omega dt} = \lim_{r \rightarrow \infty} r^2 T^r{}_t, \quad (5.11)$$

and we can write

$$\frac{d^2 E^\infty}{d\Omega dt} = \lim_{r \rightarrow \infty} \frac{\mu^2 r^2}{8\pi} f(r) \left\{ \partial_r \psi \partial_t \psi^* + \partial_t \psi \partial_r \psi^* \right\}. \quad (5.12)$$

By expanding the scalar field in the usual basis of spherical harmonics, we find

$$\frac{dE^\infty}{dt} = \lim_{r \rightarrow \infty} \frac{\mu^2}{8\pi} \sum_{l,m} r^2 f(r) \left\{ \partial_r \psi_{lm} \partial_t \psi_{lm}^* + \text{c.c.} \right\},$$

where we have already integrated over the sphere and leveraged the orthogonality property for $Y_{l,m}(\theta, \phi)$. In this expression, ψ_{lm} (and its complex conjugate), is indeed the time domain solution of the KG equation we derived in Eq. (3.17)

The derivatives of the asymptotic fields are simply

$$\partial_t \psi_{lm}(t, r \rightarrow \infty) = -4\pi \sum_n (-i\omega) e^{-i\omega t} e^{i\omega r_*} \frac{Z_{lmn}^\infty}{r}, \quad (5.13a)$$

$$\partial_r \psi_{lm}(t, r \rightarrow \infty) = -4\pi \sum_n e^{-i\omega t} Z_{lmn}^\infty \partial_r \left(\frac{e^{i\omega r_*}}{r} \right), \quad (5.13b)$$

where

$$\partial_r \left(\frac{e^{i\omega r_*}}{r} \right) = -\frac{e^{i\omega r_*}}{r^2} + i\omega \partial_r r_* \frac{e^{i\omega r_*}}{r}, \quad (5.14)$$

with $\partial_r r_* = 1 + \frac{2GM}{r} \frac{1}{f(r)}$. Because we only care about the $1/r$ behavior, we then have

$$\begin{aligned} \partial_r \psi_{lm}(t, r \rightarrow \infty) &= -4\pi \sum_n i\omega e^{-i\omega t} Z_{lmn}^\infty \frac{e^{i\omega r_*}}{r} \\ &= -\partial_t \psi_{lm}(t, r \rightarrow \infty). \end{aligned} \quad (5.15)$$

Putting everything together, the flux assumes then the following compact expression

$$\frac{dE^\infty}{dt} = -\frac{\mu^2}{4\pi} \sum_{l,m} |\dot{\psi}_{lm}|^2, \quad (5.16)$$

where the dot is the coordinate time derivative of the scalar field.

The procedure described above can be reiterated for the angular momentum flux, by looking at the (r, ϕ) component of the stress energy tensor and we find

$$\frac{dL^\infty}{dt} = -\frac{\mu^2}{8\pi} \sum_{l,m} m \left\{ \dot{\psi}_{lm} \psi_{lm}^* + \text{c.c.} \right\} \quad (5.17)$$

$$= -\frac{\mu^2}{4\pi} \sum_{l,m} m \text{Re} \left\{ \dot{\psi}_{lm} \psi_{lm}^* \right\}. \quad (5.18)$$

In order to compute explicit expressions for the fluxes, it is crucial to perform the sum over (l, m) . However, in this case, the sum is finite and we only need to take into account a finite number of modes, namely $l = 0, \dots, 4$. Explicit expressions for the fluxes in units of ε are given below

$$\begin{aligned} \frac{dE^\infty}{dt} &= -\frac{y^4}{3} + \frac{2y^5}{3} - \frac{2}{3}\pi y^{11/2} + \frac{10y^6}{3} \\ &+ e^2 \left(-y^4 + \frac{7y^5}{3} - \frac{14}{3}\pi y^{11/2} + \frac{92y^6}{3} \right) \\ &+ e^4 \left(-\frac{15y^4}{8} + \frac{17y^5}{3} - \frac{67}{4}\pi y^{11/2} + \frac{945y^6}{8} \right), \end{aligned} \quad (5.19)$$

$$\begin{aligned} \frac{dL^\infty}{dt} &= -\frac{y^{5/2}}{3} + \frac{2y^{7/2}}{3} - \frac{2\pi y^4}{3} + \frac{10y^{9/2}}{3} \\ &+ e^2 \left(-\frac{y^{5/2}}{3} + \frac{7y^{7/2}}{6} - 2\pi y^4 + \frac{59y^{9/2}}{3} \right) \\ &+ e^4 \left(-\frac{y^{5/2}}{3} + \frac{5y^{7/2}}{3} - \frac{15\pi y^4}{4} + \frac{405y^{9/2}}{8} \right), \end{aligned} \quad (5.20)$$

where, to be consistent, we kept the same number of PN-coefficients for both fluxes. It is important to recall that this expansion must always be done as a *last* step of the calculation in order to avoid a polynomial growth in time that would generate divergent fluxes.

The usual comparisons against the circular orbit are presented in Figure 3. We further provide plots of the quantity

$$\Delta \left(\frac{d\xi^\infty}{dt} \right) = \frac{d\xi^\infty}{dt} - \frac{d\xi^\infty}{dt} \Big|_{e \rightarrow 0}, \quad (5.21)$$

where $\xi = \{E, L\}$ are presented in Eqs. (5.19) and (5.20), respectively. We see that in this case the difference with the circular limit is $\sim 10^{-7}$ for the energy flux in the domain of $e \leq 0.2$ and $u_p \geq 1/8$. In the same range of (u_p, e) , the angular momentum flux is two orders of magnitude larger.

VI. COMPARING WITH SCALAR-TENSOR THEORIES

Let us compare our Eqs. (5.19)-(5.20) with the scalar fluxes presented in Eqs. (4.12) of Ref. [28]. The relation

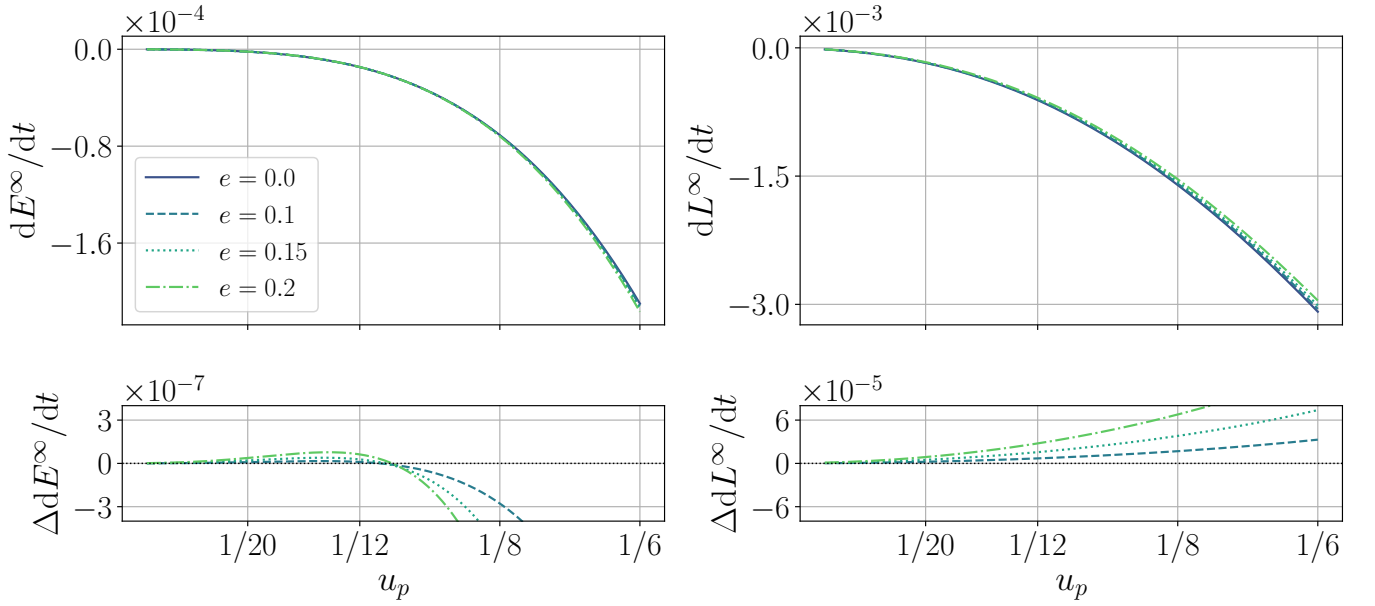


FIG. 3: We show here the energy and angular momentum flux in the first row, while in the second we show the difference with respect to the circular case. The fluxes do not differ significantly for the different values of eccentricity we chose.

between the two results is non-trivial since the orbital parametrization is different: (y, e) in our case and (x, e_t) in [28], where this choice has been made to recover trivially the circular limit.

The first step is to change variables from (y, e) to (y, e_t) , where e_t is the time eccentricity which is related to the Darwin eccentricity e via Eq. (4.38) of [76] up to third post-Newtonian order. For our purposes, we don't need to include the full expression and the 1PN correction is sufficient in the small eccentricity limit for the comparison. Hence, the relation between the two eccentricities is

$$e = e_t(1 + 3y). \quad (6.1)$$

By subsequently changing variables in our fluxes and keeping only the first two terms in the PN expansion, we get

$$\frac{d\tilde{E}^\infty}{dt} = \frac{q^2\mu^2}{M^2} \left\{ -\frac{y^4}{3} + \frac{2y^5}{3} - \left(y^4 + \frac{11y^5}{3}\right) e_t^2 - \left(\frac{15y^4}{8} + \frac{101y^5}{6}\right) e_t^4 \right\}, \quad (6.2)$$

$$\frac{d\tilde{L}^\infty}{dt} = \frac{q^2\mu^2}{M} \left\{ -\frac{y^{5/2}}{3} + \frac{2y^{7/2}}{3} - \left(\frac{y^{5/2}}{3} + \frac{5y^{7/2}}{6}\right) e_t^2 - \left(\frac{y^{5/2}}{3} + \frac{7y^{7/2}}{3}\right) e_t^4 \right\}, \quad (6.3)$$

where we have re-introduced the physical dimensions. We also point out that these expressions are equivalent to the averaged fluxes on a single orbit, i.e.

$$\left\langle \frac{d\tilde{E}^\infty}{dt} \right\rangle \equiv \frac{1}{\Delta T_r} \int_0^{\Delta T_r} dt \frac{d\tilde{E}^\infty}{dt}, \quad (6.4)$$

$$\left\langle \frac{d\tilde{L}^\infty}{dt} \right\rangle \equiv \frac{1}{\Delta T_r} \int_0^{\Delta T_r} dt \frac{d\tilde{L}^\infty}{dt}, \quad (6.5)$$

which are the quantities computed in [28].

As previously stated, the results presented in Ref. [28], in particular Eqs. (4.12), are written in terms of the couple (x, e_t) , where x differs from y by terms proportional to the symmetric mass ratio ν , namely $x = y(1 + 2\nu/3 + O(\nu^2))$ for small ν .

In order to produce a consistent check between the two results we need to perform the following identification on the notation used in Ref. [28]

$$m_1 = M, m_2 = \mu, m = m_1 + m_2 = M + \mu, \quad \nu = \frac{\mu}{M}, \delta^2 = 1 - 4\frac{\mu}{M}, s_1 = \frac{1}{2}, \quad (6.6)$$

where s_1 is the sensitivity of the Schwarzschild black hole to variations of the scalar field. Further, the sensitivity and the scalar charge are also related via

$$q = \frac{1 - 2s_2}{\sqrt{3 + 2\omega_0}}, \quad (6.7)$$

see e.g. [77]. Here, ω_0 is a ST parameter and s_2 is the sensitivity related to the second body, the scalar particle

in our case³. It is worthwhile to mention that we fix s_1 to be 1/2, i.e. its GR value, because in our investigation the central black hole is not endowed with a scalar charge.

The triple (s_1, s_2, ω_0) defines a set of unambiguous parameters that we need to use to perform the comparison. In addition to this, we also need to expand Eqs. (4.12) in Ref. [28] for small eccentricities and small symmetric mass ratio ν . This last expansion is crucial to make sure that we select only the first order in SF from the ST fluxes.

Once all these manipulations have been done, one can finally rewrite the fluxes of [28] as

$$\frac{dE^{\text{ST}}}{dt} = \frac{\nu^2 \phi_0 (1 - 2s_2^0)^2}{(3 + 2\omega_0)} \left\{ -\frac{y^4}{3} + \frac{2y^5}{3} + \left(-y^4 - \frac{11y^5}{3}\right) e_t^2 + \left(-\frac{15y^4}{8} - \frac{101y^5}{6}\right) e_t^4 \right\}, \quad (6.8)$$

$$\frac{dL^{\text{ST}}}{dt} = \frac{\nu^2 M (1 - 2s_2^0)^2}{(3 + 2\omega_0)} \left\{ -\frac{y^{5/2}}{3} + \frac{2y^{7/2}}{3} + \left(-\frac{y^{5/2}}{3} - \frac{5y^{7/2}}{6}\right) e_t^2 + \left(-\frac{y^{5/2}}{3} - \frac{7y^{7/2}}{3}\right) e_t^4 \right\}, \quad (6.9)$$

and one can immediately see the equivalence of the above relations with those shown in Eqs. (6.2) and (6.3), by comparing the content in the curly brackets.

Besides, by substituting the definition of the scalar source q in terms of sensitivities and ω_0 , we see that also the prefactor is in agreement with our findings up to a conventional multiplicative factor ϕ_0 . This comes from the normalization of the scalar field used in ST theory at infinity and can be straightforwardly set to 1. In the context of ST theory, ϕ_0 it usually comes from the requirement of having a constant value for the field at spatial infinity and it can be interpreted as a boundary condition when solving the scalar field equation.

VII. DISCUSSION AND CONCLUSIONS

In this work, we presented analytical results for a scalar charge on an eccentric orbit around a Schwarzschild black hole, using the scalar self-force (SSF) framework. The scalar field evolution is governed by the Klein–Gordon equation, which we solved in Sec. III by combining Post-Newtonian (PN) and Mano–Suzuki–Takasugi (MST) solutions. The resulting expressions preserve the periodic structure required by the orbital motion. This approach

enabled us to compute both the SF components acting on the particle in Sec. IV and the scalar radiation emitted by the system in Sec. V.

Triggered by the recent interest in characterizing binary systems in the context of scalar-tensor (ST) theories, we also performed a consistency check of our SSF results by comparing them with the analytical fluxes computed in PN approximation for ST theories (see Eq. (4.12) of Ref. [28]) in Sec. VI. By finding perfect agreement, we showed how SSF can consistently mimic the results obtained in these works once they are reduced to first-order mass-ratio corrections.

It is important to note that, in order to provide a *complete* identification of these calculations with the ST results, we would need to include the backreaction of the massive scalar field on the background geometry, which is not taken into account in our calculations. However, recent works in this direction have been performed in [38–40, 42] to investigate these classes of models with the SF approach.

Since our work is completely analytical, it would be interesting to compare our expressions to numerical simulations, in order to check which region of the parameter space can be described sufficiently well within our approach. Our results can be used to inform the scalar sector of EOB potentials for ST theories (see Ref. [32]) from SSF analytical calculations, thereby expanding the possibility to make more precise tests of GR. This would be particularly important because such EOB potentials are used to produce catalogs of simulated waveforms. These catalogs are then employed, once a GW event occurs, and to extract the physical parameters of the astrophysical sources generating the gravitational signal.

ACKNOWLEDGMENTS

The authors acknowledge the Istituto Italiano di Fisica Nucleare (INFN) iniziative specifiche QGSKY and MOONLIGHT2. SC thanks the Gruppo Nazionale di Fisica Matematica (GNFM) of Istituto Nazionale di Alta Matematica (INDAM) for the support. NM warmly thanks Miguel Zumalacárregui for insightful comments on the manuscript. NM and DU gratefully acknowledge the Max Planck Institute for Gravitational Physics (Albert Einstein Institute) in Potsdam, where this work was originally conceived. DU thanks Donato Bini, Andrea Geralico, Chris Kavanagh and David Trestini for helpful discussions and clarifications. This paper is based upon work from COST Action CA21136, Addressing observational tensions in cosmology with systematics and fundamental physics (CosmoVerse) supported by COST (European Cooperation in Science and Technology).

³ In PN theory there is no concept of primary or secondary object in the binary system. One could indeed reverse the definition of

s_1 and s_2 without any loss of generality.

-
- [1] B. P. Abbott *et al.* (LIGO Scientific, Virgo), Observation of Gravitational Waves from a Binary Black Hole Merger, *Phys. Rev. Lett.* **116**, 061102 (2016), [arXiv:1602.03837 \[gr-qc\]](#).
- [2] B. P. Abbott *et al.* (LIGO Scientific, Virgo), GW170817: Observation of Gravitational Waves from a Binary Neutron Star Inspiral, *Phys. Rev. Lett.* **119**, 161101 (2017), [arXiv:1710.05832 \[gr-qc\]](#).
- [3] J. M. Ezquiaga and M. Zumalacárregui, Dark Energy After GW170817: Dead Ends and the Road Ahead, *Phys. Rev. Lett.* **119**, 251304 (2017), [arXiv:1710.05901 \[astro-ph.CO\]](#).
- [4] P. Creminelli and F. Vernizzi, Dark Energy after GW170817 and GRB170817A, *Phys. Rev. Lett.* **119**, 251302 (2017), [arXiv:1710.05877 \[astro-ph.CO\]](#).
- [5] P. Amaro-Seoane *et al.* (LISA), Laser Interferometer Space Antenna, (2017), [arXiv:1702.00786 \[astro-ph.IM\]](#).
- [6] M. Punturo *et al.*, The Einstein Telescope: A third-generation gravitational wave observatory, *Class. Quant. Grav.* **27**, 194002 (2010).
- [7] I. Gupta *et al.*, Characterizing gravitational wave detector networks: from A[#] to cosmic explorer, *Class. Quant. Grav.* **41**, 245001 (2024), [arXiv:2307.10421 \[gr-qc\]](#).
- [8] M. Evans *et al.*, A Horizon Study for Cosmic Explorer: Science, Observatories, and Community, (2021), [arXiv:2109.09882 \[astro-ph.IM\]](#).
- [9] E. Berti *et al.*, Testing General Relativity with Present and Future Astrophysical Observations, *Class. Quant. Grav.* **32**, 243001 (2015), [arXiv:1501.07274 \[gr-qc\]](#).
- [10] J. M. Ezquiaga and M. Zumalacárregui, Dark Energy in light of Multi-Messenger Gravitational-Wave astronomy, *Front. Astron. Space Sci.* **5**, 44 (2018), [arXiv:1807.09241 \[astro-ph.CO\]](#).
- [11] N. Yunes and X. Siemens, Gravitational-Wave Tests of General Relativity with Ground-Based Detectors and Pulsar Timing-Arrays, *Living Rev. Rel.* **16**, 9 (2013), [arXiv:1304.3473 \[gr-qc\]](#).
- [12] M. Lagos, L. Jenks, M. Isi, K. Hotokezaka, B. D. Metzger, E. Burns, W. M. Farr, S. Perkins, K. W. K. Wong, and N. Yunes, Birefringence tests of gravity with multimessenger binaries, *Phys. Rev. D* **109**, 124003 (2024), [arXiv:2402.05316 \[gr-qc\]](#).
- [13] B. P. Abbott *et al.* (LIGO Scientific, Virgo), Tests of General Relativity with GW170817, *Phys. Rev. Lett.* **123**, 011102 (2019), [arXiv:1811.00364 \[gr-qc\]](#).
- [14] E. Bellini *et al.*, Comparison of Einstein-Boltzmann solvers for testing general relativity, *Phys. Rev. D* **97**, 023520 (2018), [arXiv:1709.09135 \[astro-ph.CO\]](#).
- [15] G. Cusin, M. Lewandowski, and F. Vernizzi, Nonlinear Effective Theory of Dark Energy, *JCAP* **04**, 061, [arXiv:1712.02782 \[astro-ph.CO\]](#).
- [16] J. Khoury and A. Weltman, Chameleon cosmology, *Phys. Rev. D* **69**, 044026 (2004), [arXiv:astro-ph/0309411](#).
- [17] T. Nakamura, T. Ikeda, R. Saito, N. Tanahashi, and C.-M. Yoo, Dynamical Analysis of Screening in Scalar-Tensor Theory, *Phys. Rev. D* **103**, 024009 (2021), [arXiv:2010.14329 \[gr-qc\]](#).
- [18] V. Salzano, D. F. Mota, S. Capozziello, and M. Donahue, Breaking the Vainshtein screening in clusters of galaxies, *Phys. Rev. D* **95**, 044038 (2017), [arXiv:1701.03517 \[astro-ph.CO\]](#).
- [19] L. Lombriser and A. Taylor, Breaking a Dark Degeneracy with Gravitational Waves, *JCAP* **03**, 031, [arXiv:1509.08458 \[astro-ph.CO\]](#).
- [20] J. Sakstein and B. Jain, Implications of the Neutron Star Merger GW170817 for Cosmological Scalar-Tensor Theories, *Phys. Rev. Lett.* **119**, 251303 (2017), [arXiv:1710.05893 \[astro-ph.CO\]](#).
- [21] M. Li, X.-D. Li, S. Wang, and Y. Wang, Dark Energy: A Brief Review, *Front. Phys. (Beijing)* **8**, 828 (2013), [arXiv:1209.0922 \[astro-ph.CO\]](#).
- [22] P. Jordan, *Schwerkraft und Weltall* (F. Vieweg & Sohn, Braunschweig, 1955).
- [23] M. Fierz, Über die physikalische Deutung der erweiterten Gravitationstheorie P. Jordans, *Helv. Phys. Acta* **29**, 128 (1956).
- [24] L. Bernard, Dynamics of compact binary systems in scalar-tensor theories: Equations of motion to the third post-Newtonian order, *Phys. Rev. D* **98**, 044004 (2018), [arXiv:1802.10201 \[gr-qc\]](#).
- [25] L. Bernard, Dynamics of compact binary systems in scalar-tensor theories: II. Center-of-mass and conserved quantities to 3PN order, *Phys. Rev. D* **99**, 044047 (2019), [arXiv:1812.04169 \[gr-qc\]](#).
- [26] L. Bernard, L. Blanchet, and D. Trestini, Gravitational waves in scalar-tensor theory to one-and-a-half post-Newtonian order, *JCAP* **08** (08), 008, [arXiv:2201.10924 \[gr-qc\]](#).
- [27] L. Bernard, E. Dones, and S. Mougiakakos, Tidal effects up to next-to-next-to-leading post-Newtonian order in massless scalar-tensor theories, *Phys. Rev. D* **109**, 044006 (2024), [arXiv:2310.19679 \[gr-qc\]](#).
- [28] D. Trestini, Quasi-Keplerian parametrization for eccentric compact binaries in scalar-tensor theories at second post-Newtonian order and applications, *Phys. Rev. D* **109**, 104003 (2024), [arXiv:2401.06844 \[gr-qc\]](#).
- [29] T. Damour and G. Esposito-Farese, Tensor - scalar gravity and binary pulsar experiments, *Phys. Rev. D* **54**, 1474 (1996), [arXiv:gr-qc/9602056](#).
- [30] D. Trestini, Gravitational waves from quasielliptic compact binaries in scalar-tensor theory to one-and-a-half post-Newtonian order, (2024), [arXiv:2410.12898 \[gr-qc\]](#).
- [31] S. Capozziello and A. Troisi, PPN-limit of fourth order gravity inspired by scalar-tensor gravity, *Phys. Rev. D* **72**, 044022 (2005), [arXiv:astro-ph/0507545](#).
- [32] T. Jain, P. Retegno, M. Agathos, A. Nagar, and L. Turco, Effective-one-body Hamiltonian in scalar-tensor gravity at third post-Newtonian order, *Phys. Rev. D* **107**, 084017 (2023), [arXiv:2211.15580 \[gr-qc\]](#).
- [33] T. Jain, Nonlocal-in-time effective one body Hamiltonian in scalar-tensor gravity at third post-Newtonian order, *Phys. Rev. D* **107**, 084018 (2023), [arXiv:2301.01070 \[gr-qc\]](#).
- [34] M. Shibata, K. Taniguchi, H. Okawa, and A. Buonanno, Coalescence of binary neutron stars in a scalar-tensor theory of gravity, *Phys. Rev. D* **89**, 084005 (2014), [arXiv:1310.0627 \[gr-qc\]](#).
- [35] F.-L. Julié, V. Baibhav, E. Berti, and A. Buonanno, Third post-Newtonian effective-one-body Hamiltonian in scalar-tensor and Einstein-scalar-Gauss-Bonnet gravity, *Phys. Rev. D* **107**, 104044 (2023), [arXiv:2212.13802 \[gr-qc\]](#).

- [36] C. Dyson, J. Redondo-Yuste, M. van de Meent, and V. Cardoso, Relativistic aerodynamics of spinning black holes, *Phys. Rev. D* **109**, 104038 (2024), [arXiv:2402.07981 \[gr-qc\]](#).
- [37] C. Dyson, T. F. M. Spieksma, R. Brito, M. van de Meent, and S. Dolan, Environmental effects in extreme mass ratio inspirals: perturbations to the environment in Kerr, (2025), [arXiv:2501.09806 \[gr-qc\]](#).
- [38] S. Barsanti, N. Franchini, L. Gualtieri, A. Maselli, and T. P. Sotiriou, Extreme mass-ratio inspirals as probes of scalar fields: Eccentric equatorial orbits around Kerr black holes, *Phys. Rev. D* **106**, 044029 (2022), [arXiv:2203.05003 \[gr-qc\]](#).
- [39] A. Spiers, A. Maselli, and T. P. Sotiriou, Measuring scalar charge with compact binaries: High accuracy modeling with self-force, *Phys. Rev. D* **109**, 064022 (2024), [arXiv:2310.02315 \[gr-qc\]](#).
- [40] M. Della Rocca, S. Barsanti, L. Gualtieri, and A. Maselli, Extreme mass-ratio inspirals as probes of scalar fields: Inclined circular orbits around Kerr black holes, *Phys. Rev. D* **109**, 104079 (2024), [arXiv:2401.09542 \[gr-qc\]](#).
- [41] S. Babak, J. Gair, A. Sesana, E. Barausse, C. F. Sopuerta, C. P. L. Berry, E. Berti, P. Amaro-Seoane, A. Petiteau, and A. Klein, Science with the space-based interferometer LISA. V: Extreme mass-ratio inspirals, *Phys. Rev. D* **95**, 103012 (2017), [arXiv:1703.09722 \[gr-qc\]](#).
- [42] L. Speri, S. Barsanti, A. Maselli, T. P. Sotiriou, N. Warburton, M. van de Meent, A. J. K. Chua, O. Burke, and J. Gair, Probing fundamental physics with Extreme Mass Ratio Inspirals: a full Bayesian inference for scalar charge, (2024), [arXiv:2406.07607 \[gr-qc\]](#).
- [43] S. Singh, C. E. A. Chapman-Bird, C. P. L. Berry, and J. Veitch, Revealing massive black hole astrophysics: The potential of hierarchical inference with extreme mass-ratio inspiral observations, (2026), [arXiv:2601.15198 \[astro-ph.HE\]](#).
- [44] S. H. Strub, L. Speri, and D. Giardino, Searching for extreme mass ratio inspirals in LISA: from identification to parameter estimation, (2025), [arXiv:2505.17814 \[gr-qc\]](#).
- [45] E. Poisson, A. Pound, and I. Vega, The Motion of point particles in curved spacetime, *Living Rev. Rel.* **14**, 7 (2011), [arXiv:1102.0529 \[gr-qc\]](#).
- [46] A. Pound and B. Wardell, Black hole perturbation theory and gravitational self-force [10.1007/978-981-15-4702-7-38-1](#) (2021), [arXiv:2101.04592 \[gr-qc\]](#).
- [47] I. Vega, B. Wardell, P. Diener, S. Cupp, and R. Haas, Scalar self-force for eccentric orbits around a Schwarzschild black hole, *Phys. Rev. D* **88**, 084021 (2013), [arXiv:1307.3476 \[gr-qc\]](#).
- [48] D. Bini, T. Damour, and A. Geralico, Confirming and improving post-Newtonian and effective-one-body results from self-force computations along eccentric orbits around a Schwarzschild black hole, *Phys. Rev. D* **93**, 064023 (2016), [arXiv:1511.04533 \[gr-qc\]](#).
- [49] D. Bini, T. Damour, and a. Geralico, New gravitational self-force analytical results for eccentric orbits around a Schwarzschild black hole, *Phys. Rev. D* **93**, 104017 (2016), [arXiv:1601.02988 \[gr-qc\]](#).
- [50] C. Kavanagh, A. C. Ottewill, and B. Wardell, Analytical high-order post-Newtonian expansions for extreme mass ratio binaries, *Phys. Rev. D* **92**, 084025 (2015), [arXiv:1503.02334 \[gr-qc\]](#).
- [51] D. Bini, T. Damour, and A. Geralico, High post-Newtonian order gravitational self-force analytical results for eccentric equatorial orbits around a Kerr black hole, *Phys. Rev. D* **93**, 124058 (2016), [arXiv:1602.08282 \[gr-qc\]](#).
- [52] C. Kavanagh, D. Bini, T. Damour, S. Hopper, A. C. Ottewill, and B. Wardell, Spin-orbit precession along eccentric orbits for extreme mass ratio black hole binaries and its effective-one-body transcription, *Phys. Rev. D* **96**, 064012 (2017), [arXiv:1706.00459 \[gr-qc\]](#).
- [53] D. Bini and A. Geralico, New gravitational self-force analytical results for eccentric equatorial orbits around a Kerr black hole: redshift invariant, *Phys. Rev. D* **100**, 104002 (2019), [arXiv:1907.11080 \[gr-qc\]](#).
- [54] D. Bini and T. Damour, Conservative second-order gravitational self-force on circular orbits and the effective one-body formalism, *Phys. Rev. D* **93**, 104040 (2016), [arXiv:1603.09175 \[gr-qc\]](#).
- [55] D. Bini, T. Damour, and A. Geralico, Spin-orbit precession along eccentric orbits: improving the knowledge of self-force corrections and of their effective-one-body counterparts, *Phys. Rev. D* **97**, 104046 (2018), [arXiv:1801.03704 \[gr-qc\]](#).
- [56] C. Munna, Analytic post-Newtonian expansion of the energy and angular momentum radiated to infinity by eccentric-orbit nonspinning extreme-mass-ratio inspirals to the 19th order, *Phys. Rev. D* **102**, 124001 (2020), [arXiv:2008.10622 \[gr-qc\]](#).
- [57] C. Munna and C. R. Evans, High-order post-Newtonian expansion of the redshift invariant for eccentric-orbit nonspinning extreme-mass-ratio inspirals, *Phys. Rev. D* **106**, 044004 (2022), [arXiv:2203.13832 \[gr-qc\]](#).
- [58] C. Munna and C. R. Evans, Post-Newtonian expansion of the spin-precession invariant for eccentric-orbit nonspinning extreme-mass-ratio inspirals to 9PN and e16, *Phys. Rev. D* **106**, 044058 (2022), [arXiv:2206.04085 \[gr-qc\]](#).
- [59] C. Munna, High-order post-Newtonian expansion of the generalized redshift invariant for eccentric-orbit, equatorial extreme-mass-ratio inspirals with a spinning primary, *Phys. Rev. D* **108**, 084012 (2023), [arXiv:2307.11158 \[gr-qc\]](#).
- [60] R. Fujita and W. Hikida, Analytical solutions of bound timelike geodesic orbits in Kerr spacetime, *Class. Quant. Grav.* **26**, 135002 (2009), [arXiv:0906.1420 \[gr-qc\]](#).
- [61] G. Scharf, Schwarzschild geodesics in terms of elliptic functions and the related red shift, *J. Mod. Phys.* **2**, 274 (2011), [arXiv:1101.1207 \[astro-ph.GA\]](#).
- [62] A. Cieřlik and P. Mach, Revisiting timelike and null geodesics in the Schwarzschild spacetime: general expressions in terms of Weierstrass elliptic functions, *Class. Quant. Grav.* **39**, 225003 (2022), [arXiv:2203.12401 \[gr-qc\]](#).
- [63] L. Barack, A. Ori, and N. Sago, Frequency-domain calculation of the self force: The High-frequency problem and its resolution, *Phys. Rev. D* **78**, 084021 (2008), [arXiv:0808.2315 \[gr-qc\]](#).
- [64] S. Hopper, C. Kavanagh, and A. C. Ottewill, Analytic self-force calculations in the post-Newtonian regime: eccentric orbits on a Schwarzschild background, *Phys. Rev. D* **93**, 044010 (2016), [arXiv:1512.01556 \[gr-qc\]](#).
- [65] D. Bini, A. Geralico, C. Kavanagh, A. Pound, and D. Usseglio, Post-Minkowskian self-force in the low-velocity limit: scalar field scattering, (2024), [arXiv:2406.15878 \[gr-qc\]](#).
- [66] L. Barack and A. Ori, Mode sum regularization approach for the selfforce in black hole space-time, *Phys. Rev. D*

- [61](#), 061502 (2000), [arXiv:gr-qc/9912010](#).
- [67] L. Barack, Gravitational self force in extreme mass-ratio inspirals, *Class. Quant. Grav.* **26**, 213001 (2009), [arXiv:0908.1664 \[gr-qc\]](#).
- [68] H. Nakano, N. Sago, and M. Sasaki, Gauge problem in the gravitational selfforce. 2. First postNewtonian force under Regge-Wheeler gauge, *Phys. Rev. D* **68**, 124003 (2003), [arXiv:gr-qc/0308027](#).
- [69] M. Sasaki and H. Tagoshi, Analytic black hole perturbation approach to gravitational radiation, *Living Rev. Rel.* **6**, 6 (2003), [arXiv:gr-qc/0306120](#).
- [70] A. Heffernan, A. Ottewill, and B. Wardell, High-order expansions of the Detweiler-Whiting singular field in Schwarzschild spacetime, *Phys. Rev. D* **86**, 104023 (2012), [arXiv:1204.0794 \[gr-qc\]](#).
- [71] S. A. Teukolsky, Perturbations of a rotating black hole. 1. Fundamental equations for gravitational electromagnetic and neutrino field perturbations, *Astrophys. J.* **185**, 635 (1973).
- [72] W. H. Press and S. A. Teukolsky, Perturbations of a Rotating Black Hole. II. Dynamical Stability of the Kerr Metric, *Astrophys. J.* **185**, 649 (1973).
- [73] S. A. Teukolsky and W. H. Press, Perturbations of a rotating black hole. III - Interaction of the hole with gravitational and electromagnetic radiation, *Astrophys. J.* **193**, 443 (1974).
- [74] D. Bini, G. Carvalho, and A. Geralico, Scalar field self-force effects on a particle orbiting a Reissner-Nordström black hole, *Phys. Rev. D* **94**, 124028 (2016), [arXiv:1610.02235 \[gr-qc\]](#).
- [75] M. Bianchi, D. Bini, and G. Di Russo, Scalar waves in a topological star spacetime: Self-force and radiative losses, *Phys. Rev. D* **111**, 044017 (2025), [arXiv:2411.19612 \[gr-qc\]](#).
- [76] E. Forseth, C. R. Evans, and S. Hopper, Eccentric-orbit extreme-mass-ratio inspiral gravitational wave energy fluxes to 7PN order, *Phys. Rev. D* **93**, 064058 (2016), [arXiv:1512.03051 \[gr-qc\]](#).
- [77] C. Palenzuela, E. Barausse, M. Ponce, and L. Lehner, Dynamical scalarization of neutron stars in scalar-tensor gravity theories, *Phys. Rev. D* **89**, 044024 (2014), [arXiv:1310.4481 \[gr-qc\]](#).